This is the peer-reviewed, final accepted version for American Mineralogist, published by the Mineralogical Society of America.
The published version is subject to change. Cite as Authors (Year) Title. American Mineralogist, in press.
DOI: https://doi.org/10.2138/am-2020-7385. http://www.minsocam.org/

Revision 1

Crystal-chemistry and thermal behavior of Fe-carpholite: a case of study from the Pollino Massif (southern Italy)

Ernesto Mesto[1], Salvatore Laurita[2], Maria Lacalamita[1], Rosa Sinisi[2],

Giovanna Rizzo[2], Emanuela Schingaro[1*], Giovanni Mongelli[2]

[1]Dipartimento di Scienze della Terra e Geoambientali, Università di Bari Aldo Moro, via Orabona, 4, 70125 Bari, Italy

[2]Dipartimento di Scienze, Università degli Studi della Basilicata, viale Ateneo Lucano 10, 85100 Potenza, Italy

*Corresponding author: Emanuela Schingaro, e-mail: *emanuela.schingaro@uniba.it*

RUNNING TITLE: Crystal-chemistry and thermal behavior of Fe-carpholite

ABSTRACT

The crystal chemistry and the thermal evolution of Fe-carpholite from the Pollino Massif have been investigated by means of a multimethodic approach. A combination of optical microscopy, Secondary Electron Microscopy (SEM) analyses, μRaman spectroscopy, thermal analysis (Differential Thermal Analysis, DTA; Thermogravimetry, TG), room temperature Single Crystal X-Ray Diffraction (SCXRD) and i*n situ* High Temperature X-Ray Powder Diffraction (HT XRPD) was employed.

Field and micromorphological observations showed that the studied carpholite occurs in veins embedded in fine grained matapelites and is associated to quartz, calcite, chlorite and phengite. Tiny carpholite crystals are closely associated with quartz suggesting simultaneous formation.

Structure refinements from single crystal X-ray diffraction confirm that carpholite crystallizes in the *Ccce* space group. Anisotropic refinements converged at $2.3 \leq R\ (\%) \leq 2.6$ and provided unit cell parameters $a \sim 13.77$ Å, $b \sim 20.16$ Å and $c \sim 5.11$ Å and V ~ 1419 Å^3. X_{Fe} (i.e. the molar fraction $Fe^{2+}/(Mg+Fe^{2+}+Mn)$) ~ 0.6 was derived from the refined occupancy at the M1 site and is correlated to the lattice expansion mainly along the *b* and *a* axes and to geometrical distortions of the M1, M2 and M3 octahedra. μRaman spectrum of unoriented Fe-carpholite crystals evidenced a dense succession of bands in the 200-1200 cm^{-1} spectral region as well as a strong peak at 3630 cm^{-1} and a weak peak at 3593 cm^{-1} which account for the presence of two independent OH groups also provided by the structure refinement.

The TG curve indicates a total mass loss of 15.6% in the range 30-1000°C whereas the DTA curve showed a broad endothermic band at ~ 400°C, extending up to ~ 650°C and weak exothermic peaks at ~700 and 750°C. The latter may be ascribed to the breakdown of the Fe-carpholite structure and crystallization of new phases. The *in situ* high temperature X-ray powder diffraction, allowed to follow the pattern evolution in the temperature range from 30 to 1105°C. Rietveld refinements were carried

out for all patterns collected from 30 to 630°C. No significant modifications were observed from 30 to 355°C whereas reflection splitting appeared starting from 380°C as a consequence of a Fe-oxidation/deprotonation process. The carpholite and the deprotonated carpholite phases coexist in the 380-580°C temperature range whereas the only deprotonated phase is observed up to 630°C. Above this temperature the carpholite structure collapses and the characteristic peaks of spinel and quartz phases are observed. At 1105°C, spinel, mullite, garnet, cristobalite and tridymite may be clearly identified. The present work contributes to fill the gap on the thermal stability of Fe-carpholites and may have implications for a better understanding of the thermal evolution of H*P*/L*T* metasediments.

Keywords: Fe-carpholite, crystal-chemistry, thermal evolution, SEM, SCXRD, HT XRPD, thermal analysis, μRaman spectroscopy

This is the peer-reviewed, final accepted version for American Mineralogist, published by the Mineralogical Society of America.
The published version is subject to change. Cite as Authors (Year) Title. American Mineralogist, in press.
DOI: https://doi.org/10.2138/am-2020-7385. http://www.minsocam.org/

INTRODUCTION

The carpholite group encompasses hydrated inosilicates with general formula $A_{0-1}M1_2M2_2M3_2[(OH, F)_4(Si_2O_6)]_2$ where *A* = [], K, Ba and Na, *M1* = Mn, Mg, Fe, Al, Li and Na, *M2* = Al, V^{3+}, Fe^{3+} and Ti, and *M3* = Al, Mg, V^{3+}, Fe^{3+} and Ti (Basso and Carbone 2010). These minerals have a trellis structure based on pyroxene-like I-beam units $[Al_2Si_4O_{16}(OH, F)_4]^{14-}$ which are connected to side-ribbons defining two different open channels running along the *c* direction. One of them hosts the *A* site, with dodecahedral coordination, that may be empty or partially occupied by large cations. Similarities of this structure topology with that of the magbasite were recently described by Welch et al. (2014).

Carpholites have been studied from the point of view of their mineral chemistry by several authors since the first half of the 20th century (e.g. MacGillavry et al. 1956; Naumova et al. 1975; Goffé 1980; Theye et al. 1992; Oberhänsli et al. 2001; Agard et al. 2005; Escuder-Viruete et al. 2011; Vitale et al. 2013 and references therein; Pourteau et al. 2014). From a crystal structure viewpoint, a complete description of carpholite, $[]MnAl_2Si_2O_6(OH)_4$, was provided by Lindeman et al. (1979), whereas the potassic-carpholite, (K, [])(Li, Mn)$Al_2Si_2O_6(OH, F)_4$, was described by Ghose et al. (1989) and Tait et al. (2004). Basso et al. (2005) published the structure refinement of vanadiocarpholite, [] Mn(V^{3+}, Al)$_2Si_2O_6(OH)_4$, whereas, although the unit cell parameters of Fe-, Mg-carpholites, [](Fe, Mg) $Al_2Si_2O_6(OH)_4$, are reported in different studies (Mottana and Schreyer 1977; Steen and Bertrand 1977; Viswanathan and Seidel 1979; Goffé 1980; Bertoldi et al. 2006), structure refinements on these specimen are present in few papers (see Viswanathan 1981; Ferraris et al. 1992; Fuchs et al. 2001). Finally for balipholite, Ba(Al, Li)$AlMgSi_2O_6(OH)_4$, Peng et al. (1987) only report unit cell parameters.

The crystal structure of carpholite was solved in the *Ccce* (previously *Ccca*) space group. In some works, a few reflections violating the space group symmetry were detected for the Fe-, Mg-carpholite

(see Mottana and Schreyer 1977; Ferraris et al. 1992; Fuchs et al. 2001), pointing to a lower (monoclinic) symmetry.

Basing on the available literature data on carpholites, Basso and Carbone (2010) derived predictive equations relating lattice parameters and mean polyhedral cation-oxygen distances to the chemical composition of the octahedral sites.

Fe-Mg carpholite occurs in several belts, including the Alpine-Himalayan belt (Bousquet et al. 1998, 2008; Oberhänsli et al. 2001, 2013), the eastern Central Alps (Grisons and Engadine Window, Goffé and Oberhänsli 1992), the Arabian continental margin (Oman, Goffé et al. 1988), the Hellenides (Theye et al. 1992), the northern Apennines (Theye et al. 1997), the Menderes Massif (Oberhänsli et al. 2001), the south-eastern Betics in the Alpujarride Units of Spain (Booth-Rea et al. 2002), the Svalbard Caledonides and Spitsbergen (Agard et al. 2005), the Qilian suture zone (Song et al. 2007), Hispaniola (Escuder-Viruete et al. 2011), and Anatolia (Pourteau et al. 2014). In southern Apennines (Italy), precisely in the Pollino Massif area, the occurrence of carpholite has been reported for the first time by Busato and Giampaolo (1983) and more recently by Laurita (2009) and Vitale et al. (2013).

In the present study, the crystal chemistry of the Fe-carpholite from the Pollino Massif (Liguride Complex, Frido Unit) has been investigated by combining Secondary Electron Microscopy (SEM), Single Crystal X-Ray Diffraction (SCXRD) and μRaman spectroscopy. Differential Thermal Analysis (DTA), Thermogravimetry (TG) and i*n situ* High Temperature X-Ray Powder Diffraction (HT XRPD) experiments were also carried out in order to evaluate the thermal behavior of the studied Fe-carpholite. To the best of the authors knowledge, this is the first *in situ* study of the Fe-carpholite evolution, since only one *ex situ* high temperature diffraction study of a carpholite has been so far reported (Aoki 1966).

MATERIALS AND METHODS

This is the peer-reviewed, final accepted version for American Mineralogist, published by the Mineralogical Society of America.
The published version is subject to change. Cite as Authors (Year) Title. American Mineralogist, in press.
DOI: https://doi.org/10.2138/am-2020-7385. http://www.minsocam.org/

Geological setting and sampling

The southern Apennines chain is mainly composed of Mesozoic-Tertiary sedimentary rocks derived from the former Apulian passive margin, overlain by Pliocene-Pleistocene terrigenous deposits (Cello and Mazzoli 1998; Patacca and Scandone 2007). The Liguride Complex (Tortorici et al. 2009; Vitale et al. 2013) cropping out in the Pollino Massif (Fig. 1A) has been subdivided into two units, the metamorphosed Frido Unit and the non-metamorphic North Calabria Unit (Bonardi et al. 1988). The Frido Unit represents the uppermost part of the Liguride Complex (Cavalcante et al. 2009; Tortorici et al. 2009) and consists of a metamorphosed sedimentary sequence with oceanic and continental type rocks (Knott 1987, 1994; Spadea 1979, 1982; Laurita et al. 2104; Dichicco et al. 2018; Rizzo et al. 2018). The oceanic bodies are mainly represented by large slices of serpentinized peridotites (Dichicco et al. 2015, 2017) containing dismembered metadolerite dykes and metabasalts (Spadea 1982; Sansone and Rizzo 2012; Sansone et al. 2011, 2012a, 2012b; Laurita and Rizzo 2018; Rizzo et al. 2019). The metasedimentary cover consists either of metapelites, metarenites, quarzites and isolated bodies of metalimestones and calcschists (Monaco et al. 1995; Rizzo et al. 2016).

The studied carpholite comes from fine-grained greyish metapelites with cataclastic to mylonitic texture cross cut by quartz and quartz–carbonate veins cropping out in Fosso Santo Ianni, close to Viggianello (Potenza, Fig. 1B, 1C). In the field, carpholite is usually observed in quartz and quartz-calcite veins as mesoscopic greenish hair-like fibres up to 15-20 cm in length (Fig. 1D).

Optical microscopy and SEM-EDS observations

Samples were studied using conventional optical microscopy and SEM-EDS imaging. Micromorphological analysis was undertaken using scanning electron microscopy and a XL30 Philips LaB_6 ESEM instrument equipped with an energy dispersive X-ray spectrometer (SEM–EDS) operating

This is the peer-reviewed, final accepted version for American Mineralogist, published by the Mineralogical Society of America.
The published version is subject to change. Cite as Authors (Year) Title. American Mineralogist, in press.
DOI: https://doi.org/10.2138/am-2020-7385. http://www.minsocam.org/

at beam current of 1 μÅ and an accelerating voltage of 15 kV at the Department of Sciences, University of Basilicata, Italy.

SCXRD

Two single crystals selected for the good diffraction behavior (hereafter labelled Carph4_1 and the Carph4_3) were used for X-ray data collection on a Bruker AXS APEX II diffractometer with kappa-geometry installed at the Earth and Geoenvironmental Department, University of Bari, and equipped with a monochromatized MoKα-radiation and a APEX II CCD detector. A combination of several ω and φ rotation sets with 0.5° frame scan width, with 30 seconds acquisition time for each frame and with a crystal-to-detector distance of 4 cm was used. A sphere of three-dimensional data was explored by optimizing the collection strategy by the Apex program suite (Bruker 2010). Data reduction, including intensity integration, correction for Lorentz and polarization effects, was done using the software SAINT (Bruker 2007). Empirical absorption corrections were applied to all data on the basis of the intensities of equivalent reflections by means of multi-scan method implemented in SADABS (Bruker 2009). Subsequent analysis of the intensity data by XPREP (Sheldrick 2008) indicated that the distribution of the normalized structure factors is centrosymmetric. The reflection conditions allowed to assign the *Ccce* symmetry to the studied crystals. In detail, reflections analysis for the Carph4_1 sample showed the presence of 1607 violating the *e* glide out of which 43 reflections have $I > 3\sigma(I)$. Similarly, 764 measured reflections violating systematic absences has been found for the Carph4_3 crystal, but none with $I > 3\sigma(I)$. The inspection of the simulated precession images on the *hk*0 and *hk*1 levels allowed to ascertain that these reflections are actually experimental artefacts (see the Supplemental Figs. S1a and S1b).

This is the peer-reviewed, final accepted version for American Mineralogist, published by the Mineralogical Society of America.
The published version is subject to change. Cite as Authors (Year) Title. American Mineralogist, in press.
DOI: https://doi.org/10.2138/am-2020-7385. http://www.minsocam.org/

In addition, the structure solution obtained by SUPERFLIP software (Palatinus and Chapuis 2007) confirmed the *Ccce* space group. The structure refinement was performed using the program CRYSTALS (Betteridge et al. 2003) starting from the atomic parameters derived by the structure solution step. Atom labeling was after Fuchs et al. (2001). Reflections with $I > 3\sigma(I)$ were used for the structure refinement. Refined parameters were: atomic positions, anisotropic atomic displacement parameters, the overall scale factor and Mg/Fe occupancies. After convergence, a difference Fourier map was calculated in order to locate the H atom positions. The latter were introduced in the refinement and treated with a riding model. The difference Fourier map also showed a very weak residual peak in the A cavity, corresponding to the expected position of the K-site in Ghose et al. (1989) but its intensity (0.4 $e^-/Å^3$) was considered too low to be modeled in the refinement. The crystal data, data-collection information and refinement details are listed in Table 1, atomic positions and displacement parameters are listed in Table 2 while the relevant geometrical parameters are given in Table 3.

µRaman spectroscopy

The µRaman spectroscopy analysis was carried out at the Department of Sciences, University of Basilicata, using a HORIBA Jobin-Yvon LabRamHR800 spectrometer equipped with a HeNe laser source characterized by wavelength of 633 nm, a multichannel electronically cooled CCD detector operating at -70 °C, an edge filter that exclude from detection shift below 150 cm^{-1} and a computer-controlled motorized x-y-z stage. Raman spectra have a spectral resolution of 4 cm^{-1} that was obtained by a holographic grating of 600 lines/mm. Prior to the measurements, the laser beam was centered and the spectrometer calibrated by checking the position of the first-order signal produced by a synthetic Si standard (at ± 520.7 cm^{-1}). The spectrometer, coupled to an Olympus optical microscope, operated in

confocal mode in order to improve both the focus of laser beam on sample surface and the collection of the generated Raman signal. A laser beam spatial resolution of 1 μm was obtained using the 100× objective. The spectra were measured in the 200-1800 cm^{-1} and 3400-3800 cm^{-1} regions and resulted from the average of 5 acquisitions of 10 s each to optimize the signal/noise ratio.

Thermal analysis

Simultaneous differential thermal, thermogravimetric and derivative thermogravimetric analysis (DTA/TG/DTG) was carried out using a Toshiba STA7200RV analyzer. The measurement was performed on about 17 mg of carpholite placed in an alumina crucible and heated from room temperature up to 1000°C at a rate of 10°C/min in air.

***In situ* HTXRPD**

High-temperature X-ray powder diffraction data were collected in air using a Panalytical Empyrean X-ray diffractometer with Bragg-Brentano geometry, large beta filter-Nickel, detector (PIXcel3D) and CuKα radiation, and operating at 40 kV/40 mA. The instrument, installed at the Earth and Geoenvironmental Department, University of Bari, was equipped with an Anton Paar HTK 1200N high-temperature chamber. The powder was deposited on a corundum sample holder. The X-ray data were collected in the 2θ range 5-85° (step size 0.013°, scan speed 0.067 °/s) from 30° to 1105°C. The temperature step on heating rate was 10°C/min and the equilibration time at every 25°C temperature step was 15 min. A total of 44 XRPD patterns were recorded, each pattern consisting of 6093 experimental points. At each temperature 3 repeated scans were measured, about 20 minute each, and then summed (total collection time at each temperature about 1 hour). The diffraction patterns were processed using the PANalytical B.V. software HIGHScore Plus version 3.0e. Rietveld refinements

were performed using the *Ccce* space group using the GSASII software (Toby and Von Dreele 2013). The refined parameters at each temperature were: scale factors, zero shift and lattice parameters. Atomic coordinates and equivalent isotropic-displacement parameters were not allowed to vary. The background was modeled using a Chebychev polynomial approximation of 15th order, whereas the peak profile was described by a pseudo-Voight. The refined cell parameters at each temperature are listed in Table 5. For the protonated Fe-carpholite ("c" phase in Table 5) the starting cell parameters (a = 13.7656(4) Å, b = 20.1426(6) Å, c = 5.1122(2) Å) and structural model were those of the RT single crystal structure refinement for the sample Carph4_1. For the deprotonated carpholite ("dc" phase in Table 5) the starting cell parameters (a = 13.7571(6) Å, b = 20.2571(9) Å, c = 5.1357(2) Å) and structural model were those refined for the Carph4_1 *in situ* single crystal heated at 550°C (Mesto et al., unpublished data, see also the Thermal behavior of Fe-carpholite section of the manuscript). The sequential refinement procedure implemented in GSASII was employed by using: only the "c phase" from RT to 355°C; the "c phase" plus the "dc phase" from 380 to 580°C; only the "dc phase" at 605°C and 630°C.

RESULTS AND DISCUSSION

Petrography and microchemistry

Metapelites are mainly composed of quartz + phengite + stilpnomelane + chlorite + calcite + albite + epidote. Two types of phengites can be distinguished: 1) large minerals without preferred orientation, likely of detrital origin, and 2) fine-grained micas usually associated to chlorite. Epidote and apatite occur as accessory minerals.

Metapelites also contain lens shaped quartz and quartz-calcite veins with micrometric to millimetric sizes. The mineralogical composition of veins includes quartz, calcite, and carpholite. Chlorite and

This is the peer-reviewed, final accepted version for American Mineralogist, published by the Mineralogical Society of America.
The published version is subject to change. Cite as Authors (Year) Title. American Mineralogist, in press.
DOI: https://doi.org/10.2138/am-2020-7385. http://www.minsocam.org/

phengite may also be present. In veins, carpholite mostly appears as typically hair-like 200-300 μm long thin fibers as well as isolated tiny needles embedded in quartz crystals (Figs. 2A and 2B). Carpholite is green or pale yellow in color, with light brown pleochroism. The expected parallel extinction under crossed polarizers was observed. This mineral also grows as aggregates of crystals developed along *c* axes (Figs. 2C and 2D). Chlorite forms crystals parallel to the carpholite showing equilibrium textures. Quartz is closely associated with tiny carpholite crystals suggesting simultaneous formation (Figs. 2E and 2F).

The EDS spectrum evidenced the presence of Si, Al, Fe, Mg and subordinately of Ti and Mn (see the inset in Fig. 2C). Variations in carpholite composition are not significant and inner parts display a homogeneous composition in comparison to crystal rims in agreement with the chemical data from electron microprobe analysis in Vitale et al. 2013 (their Table 1). In detail, these authors documented a homogeneous, Fe-rich and Mn-poor carpholite in the Frido Unit metapelite with X_{Fe} (i.e. molar $Fe^{2+}/(Mg+Fe^{2+}+Mn)$) varying from 0.57 to 0.69. Similar values of Fe/(Fe+Mg) content (0.61 to 0.63) were derived from the refined occupancies of the studied Carph4_1 and Carph4_3 crystals, respectively. The chemical formulae of the studied crystals are reported in Table 4 in comparison to those of other carpholites in the literature for which structure refinement was available. In the Mg-Mn-Fe ternary diagram of Figure 3, the studied crystals and the Vitale et al. (2013) samples plot very close to the Mg-Fe join and exhibit Fe content slightly lower than those of the Fe-carpholites in Bertoldi et al. (2006), Ferraris et al. (1992) and Mottana and Schreyer (1977).

Crystal structure and crystal-chemistry of Fe-carpholite

In previous literature, the symmetry of carpholite was debated, due to the observation of symmetry violating reflections, in association to optical and spectroscopic anomalies (Ferraris et al. 1992; Fuchs

et al. 2001). In particular, Ferraris et al. (1992) hypothesized that the real symmetry of carpholite was monoclinic and was associated to order/disorder distribution of hydrogen, OH-F or $OH\text{-}O^{2-}$ substitution, Fe/Mg ordering or impurities in the A site. Fuchs et al. (2001) concluded that short range ordering in carpholites, as revealed by FTIR and Raman spectroscopies, could result in a number of extra OH stretching bands, suggesting symmetry lowering, in contrast with X-ray diffraction. In our study, a close inspection of the simulated *hk*0 layer allowed to assess that the low intensity reflections violating the *e* glide plane are artefacts generated by the occurrence of powder ring-like features intersecting the position of the forbidden reflections (see the Supplemental Fig. S1a). Lack of oblique extinction as well as of extra OH-stretching band in the Raman spectra (see below) are also observed. Therefore, the structural model in *Ccce* space group represents an adequate description of the Fe-carpholite from Frido Unit.

The refined unit cell parameters and volume for the studied carpholite are: $a \sim 13.77$ Å, $b \sim 20.16$ Å, $c \sim 5.11$ Å and $V \sim 1419$ Å^3 (Table 1). In the crystal structure, there are: one symmetry independent tetrahedron; three symmetry independent octahedra (M1, M2 and M3); two hydrogen positions (H1 and H2), see Table 2. The M1 octahedron is Mg, Fe-centered whereas the M2 and M3 octahedra are Al-centered. The M2 octahedra are sandwiched between two pyroxene-like single silicate chains forming the known pyroxene I-beam unit which run parallel to *c*. In turn, the I-beam units are connected through three edge-sharing M1 and M3 octahedra in a zig-zag like fashion (Figs. 4a and 4b). The M1 and M3 octahedra also form walls running parallel to *c*. Two cavities may be distinguished: the smallest is defined by four octahedra (two M1 and two M2) and hosts the A site; the largest results from four tetrahedra which are connected to M1 and M3 octahedra (Fig. 4). The latter cavity host the hydroxyl groups OH(2) extending from the M1-M3 ribbons and lying in the *ab* plane (Figs. 4 and 7). The other hydroxyl, OH(1), is also shown in Figure 7 and is almost parallel to the *c* axis. Bond strength

This is the peer-reviewed, final accepted version for American Mineralogist, published by the Mineralogical Society of America.
The published version is subject to change. Cite as Authors (Year) Title. American Mineralogist, in press.
DOI: https://doi.org/10.2138/am-2020-7385. http://www.minsocam.org/

balance (Brown and Altermatt 1985; Brown 2002) is reported in Supplemental Table S1 and refers only to the carph4_1 sample because similar values are also obtained for carph4_3 crystal. It is confirmed that only the OH(2) hydroxyl is involved in hydrogen bonding with the acceptor atom O3 (Ferrari et al. 1992; Fuchs et al. 2001). X-ray scattering refinement provided an M1 occupancy of ~38% Mg and ~62% Fe (Table 2) which corresponds to X_{Fe} = 0.6. Figure 5 shows the relationships between the X_{Fe} and the cell parameters for the studied and literature carpholites. Some trends are better evidenced when referred only to Fe-, Mg-carpholite, i.e. if some samples from the literature (i.e. carpholite of Mottana and Schreyer 1977, and Lindemann et al. 1979; vanadiocarpholite of Basso et al. 2005; potassic-carpholite of Ghose et al. 1989, and Tait et al. 2004; balipholite of Peng et al. 1987) are excluded. In particular, it is evident that the lattice expansion along the *b* and *a* axes, is affected by the ionic radius of the atom species at the M1 site (Mg, Fe or Mn), expanding the ribbons along [010] and [100] but not along [001] and corresponds to an increased substitution of Fe^{2+} for Mg at the M1 site in most literature samples. However, further substitutions at M1 (Mn, V, etc) can also have even larger effect (samples at lower X_{Fe} in Figs. 5a and 5b). This feature was also reported by Viswanathan and Seidel (1979). The occupancy of the A site, instead, seems to mostly influence the length of the *b* lattice parameter (see Fig. 5b, samples from Mottana and Schreyer 1977; Peng et al. 1987; Ghose et al. 1989; Tait et al. 2004; Basso et al. 2005). The *c* parameter is unaffected by X_{Fe} (Fig. 5c). The above cell parameters variations are reflected, although to different extent, in the geometrical variation of the octahedra (M1, M2 and M3) of carpholite structure. Regarding the M1 site, note that the <M1-O> distances of the Fe-carpholites (Carph4_1 and Carph4_3 crystals in this study and the Oman sample in Ferraris et al. 1992) are slightly longer than those of the Mg-carpholites in Viswanathan (1981) and Fuchs et al. (2001), see Table 3. On the other hand, the <M1-O> distances of the Mg-, Fe-carpholites (~2.13 Å, Table 3) are shorter than those (~2.18 Å, Table 3) of carpholite, vanadiocarpholite and

This is the peer-reviewed, final accepted version for American Mineralogist, published by the Mineralogical Society of America.
The published version is subject to change. Cite as Authors (Year) Title. American Mineralogist, in press.
DOI: https://doi.org/10.2138/am-2020-7385. http://www.minsocam.org/

potassic-carpholites (in Lindemann et al. 1979; Basso et al. 2005; Ghose et al. 1989, respectively) as expected from the difference in the ionic radii of the central cations in the M1 octahedron. The variation of the chemical composition of the M1 site among the studied and the literature samples (see Table 4) is also reflected by the values of the M1 bond length distortion parameter (BLD_{M1} parameter in Table 3) which ranges between 4.01 and 5.78. Note that the cation substitutions at the M1 site differently affect the M3 and M2 polyhedra, which are both generally occupied by only Al^{3+} cations (see Table 4 and Fig. 4). Indeed, all the carpholites in Table 3 show <M3-O> distance ~ 1.90 Å and low variability of the BLD_{M3} parameter (~ 2.29÷2.57) with the exception of the VC sample in Basso et al. (2005). For this sample the values of the <M3-O> (1.938 Å) and BLD_{M3} (2.175) are a consequence of the greatest amount of $Al^{3+} \leftrightarrow V^{3+}$ substitution in the site. The <M2-O> distance instead shows a remarkable variability (~1.88÷1.98 Å) among all the carpholites (Table 3). The same trend is observed for the BLD_{M2} parameter (~ 2.51÷6.32) compared to the BLD_{M3} one (Table 3). However, the geometry of the M2 site may also be affected by the chemical composition of the A-site. Analysis of the O4-O4 distances in Table 3 evidences that there is not a clear correlation between the size of the channel and the A-site occupancy. However, the potassic-carpholite of Ghose et al. (1989) which contains the highest amount of K^{+} (0.35 apfu), shows the lowest value of the O4-O4 distance (3.617 Å, Table 3). Table 3 also reports the values of the L/S parameter which is the ratio between the longest (O2-O2 distance) and shortest (O3-O3 distance) diagonals of the eight-membered channel and expresses the size of the largest cavity (see Fig. 4a). As expected, the studied and literature Fe-, Mg-carpholites show an L/S ratio (~ 1.76) higher than those (~1.66÷1.71) of the pure carpholite (Lindemann et al. 1979) and of the vanadio- and potassic-carpholites (in Basso et al. 2005; Ghose et al. 1989, respectively). Indeed, the largest the M1 and M3 octahedra, the smallest the L/S ratio, as the increase of ionic radii of cations

This is the peer-reviewed, final accepted version for American Mineralogist, published by the Mineralogical Society of America.
The published version is subject to change. Cite as Authors (Year) Title. American Mineralogist, in press.
DOI: https://doi.org/10.2138/am-2020-7385. http://www.minsocam.org/

at the M1 and M3 sites mostly enlarges the *b* lattice parameter (Fig. 5b) and therefore lengthens the O3-O3 distance.

Hydrogen speciation

Several unoriented crystals of carpholite were examined by Raman micro-spectroscopy at room temperature. Representative μRaman spectra, at low (200-1200 cm^{-1}) and high (3400-3800 cm^{-1}) frequency, are displayed in Figure 6a and 6b, respectively. No signals were found in the 1400-1800 cm^{-1} interval and the relevant spectrum was not shown. As to the low frequency spectrum, our results well fit the Raman shift data retrieved from the RRUFF Raman spectroscopy database (RRUFF ID: R060608). In particular, the Raman pattern of the studied Fe-carpholite consists of a close succession of bands distributing throughout the 200-1200 cm^{-1} spectral region. The characteristic Raman bands in the 1100-740 cm^{-1} region (at ~ 747, 886, 928, 969, 1042, 1092 cm^{-1}) are due to stretching Si-O-Si vibrations; the bands at 566 and 617 cm^{-1} may be attributed to out-of-plane bending OH vibrations; the bands at ~ 480 and 449 cm^{-1} may be ascribed to Al-O vibrations of the AlO_6 octahedra, whereas the strong band at 411 cm^{-1} and the other bands at lower wavenumbers (i.e. at ~ 220, 287, 322, 356 cm^{-1}) may depend mainly on the Mg-O and Fe-O vibrations of the MO_6 octahedra. This assignment is in agreement with that reported in Makreski et al. (2006) for the Vrpsko carpholite and for other pyroxenes and pyroxenoids from Macedonia.

Regarding the high frequency, the spectrum of the studied Fe-carpholite is made up of a strong peak at 3630 cm^{-1} and a weak peak at 3593 cm^{-1} which account for the presence of two independent OH groups as also derived by the structure refinement. Following the results of polarized Raman spectroscopy on the ML and MA magnesiocarpholite in Fuchs et al. (2001), the 3630 cm^{-1} peak may be attributed to vibration of the O-H(1) vector which is almost parallel to the *c* axis whereas the 3593 cm^{-1}

peak may be due to vibrations of the O-H(2) vector which lies in the *ab* plane (see Fig. 7). Similar results were reported for the Fe-carpholite in Ferraris et al. (1992) although the authors also observed a third weak band at 3570 cm^{-1}. Fuchs et al. (2001), instead, found different Raman and FTIR spectra for different carpholite crystals. Those authors tried to explain the discrepancies between Raman and XRD results (their carpholite showed *Ccce* symmetry) by invoking short range ordering due to local arrangements of point defects.

Thermal behavior of Fe-carpholite

The curves from the TG-DTA-DTG experiment are shown in Figure 8. The TG curve provides a total mass loss of 15.6% of the studied Fe-carpholite. The constant mass loss (~ 2%) in the TG curve up to 550°C can be mainly due to the sample separation method (hand picking under the binocular microscope). Indeed, the acicular carpholite crystals can contain some grains of the finely intergrown matrix, that, in turn, may contribute to the observed decomposition (see also Kusiorowski et al. 2015). The DTA curve evidences a very broad effect around 400°C and additional weak endothermic peaks at 705 and 740°C. The first effect could also be due to a progressive carpholite deprotonation process, proceeding up to about 650°C, whereas the other features may be related to the decomposition of impurities, likely due to the occurrence of a small carbonate component. Very weak exothermic peaks are also observed at ~700 and 750°C. These peaks may be associated to the breakdown of the Fe-carpholite and crystallization of new phases. No well defined peaks may be identified above 750°C. Note that only one TG-DTA is available in the literature for the Fukuzumi mine carpholite with chemical formula $(Mn_{0.89}Fe^{2+}_{0.15})(Fe^{3+}_{0.07}Al_{1.91})(Al_{0.09}Si_{1.19})O_{5.91}(OH)_{4.09}$ (Aoki 1966). The author reported broad endothermic peaks at 230 and 712°C and sharp peaks at 850, 870 and 925°C. Probable

exothermic peaks at 770, 817, 903 and 979°C were also identified. The different band positions reflect the different mineral chemistry of the carpholites.

The room temperature XRPD pattern of the studied carpholite matches that of the ferrocarpholite in the PDF database (98-007-2894 PDF number). The Rietveld refinement of the RT pattern, obtained starting from the structure model of the single crystal X-ray diffraction, is shown in Supplemental Figure S2. Rietveld refinements were performed for all patterns from 30 to 630°C and provided agreement factors, R_{wp}, in the range from 9 to 25%. Unit cell parameters similar to those derived from single crystal structure refinement were obtained (see Table 5).

No modifications are observed in the diffraction patterns of carpholite collected from 30 to 355°C (see Fig. 9a) whereas a splitting of the reflections into two separate peaks occurs starting from 380°C and progressing up to 580°C. The splitting is particularly evident, for instance, for the reflections at 2θ ~ 17.7° (040 reflection) and at 26.5° (060 reflection), see the blue arrows in the Figure 9a. At 605° these reflections appear broadened and shifted to respectively 2θ ~ 17.8° and 26.8° (see the red arrows in the Figure 9a). This trend is consistent with the progression of the Fe-oxidation in the M1 site and the consequent deprotonation process. Therefore, in the 380-580°C temperature range the carpholite and the deprotonated carpholite phases coexist (see Table 5). Starting from 605 to 630°C (Figs. 9a and 9b), only the deprotonated carpholite is present. Above 630°C the structure of the deprotonated carpholite collapses and new phases crystallize in a two-step reaction starting from about 680°C. In detail, the pattern collected at 680° contains only the characteristic peaks of spinel whereas at 780°C the *β*-quartz reflections may be identified (Fig. 9b). This suggests that under the adopted experimental conditions Fe-carpholite may dissociate according to the following idealized reaction scheme:

$$FeAl_2Si_2O_6(OH)_4 \text{ (Fe-carpholite)} \rightarrow FeAl_2O_4 \text{ (hercynite)} + 2SiO_2 \text{ (}\beta\text{-Quartz)} + 2H_2O.$$

This reaction involves a mass loss of about 11% which is in keeping with the experimental mass loss from the TG curve in the ~600-750° C range (about 13%, see Fig. 8), the difference being explained by minor impurities (see above).

By increasing the temperature up to 1030°C, new peaks begin to appear but they may be clearly ascribed to mullite, garnet, *β*-cristobalite and *β*-tridymite only in the pattern at 1105°C (Fig. 9b). This mineral assemblage results from the following reaction:

$$3FeAl_2O_4 \text{ (hercynite)} + 4SiO_2 \rightarrow Al_4SiO_8 \text{ (mullite)} + Al_2Fe_3Si_3O_{12} \text{ (almandine)}$$

These results resemble those found for the Fukuzumi mine carpholite in Aoki (1966), allowing for the evident differences in mineral chemistry. In particular, the author stated that the carpholite structure is completely destroyed at 600°C. However, the thermal evolution of the Fukuzumi mine carpholite involves a three-step reaction mechanism where: the carpholite transforms to braunite, sillimanite and quartz (step 1); the braunite and sillimanite form galaxite and quartz (step 2); galaxite and quartz transform to spessartine and mullite. Therefore, with the temperature increase, both our Fe-carpholite and the literature carpholite evolve to a mullite and garnet combination through the formation of a spinel phase.

Finally, the evolution of the unit cell parameters and resulting cell volume of the studied Fe-carpholite in the range 30-580°C is plotted in Figure 10. The data set was normalized on the basis of the lattice parameters at room temperature. From room temperature to 380°C, a slight increase of the *b* and *c* parameters and of the cell volume is observed as a consequence of the thermal expansion of the structure whereas the *a* parameter seems to be not affected by the temperature increase (Fig. 10). An

abrupt discontinuity in the trend of the *c* parameter and of the unit-cell volume occurs at 405°C and may be associated to Fe-oxidation/deprotonation process of the carpholite. The process involves a cell volume decrease of ~6% compared to that measured at RT without symmetry change. Similar structural modifications were previously reported for other inosilicates (e.g. Fe-amphiboles in Kusiorowski et al. 2015 and Oberti et al. 2018) as well as for phyllosilicates (e.g. Ventruti et al. 2008; Zema et al. 2010). In addition, preliminary results from *in situ* HT-SCXRD experiments (Mesto et al., in preparation) on the Carph4_1 sample confirm that the deprotonated carpholite has the same space group of the RT carpholite and reduced lattice parameters and cell volume. The data indicate that the Fe-oxidation/deprotonation process is associated to a shrinking of the M1 octahedron and to a migration of the its central cation towards the O(4) site which hosted the OH(1) hydroxyl. Consistently, Raman spectra of heated carpholite crystals (Mesto et al., in preparation) evidence a progressive decrease of the band associated to the stretching vibrations of the OH(1) hydroxyl which is not involved in the hydrogen bonding.

IMPLICATIONS

In recent years, Fe-Mg carpholite has gained a renewed interest as index mineral in high-pressure/low-temperature conditions for blueschist facies metapelites (Pourteau et al. 2014, and references therein) and metabasites (Agard et al. 2005). Moreover, in low temperature conditions, carpholite-bearing quartz veins may form during the transition middle to high pressure (Goffé et al. 1988; Theye et al. 1992; Agard et al. 2001; Rimmelé et al. 2003; 2005; 2006; Candan et al. 2005; Trotet et al. 2006; Song et al. 2007; Verlaguet et al. 2011; Plunder et al. 2012) in the FeO-MgO-Al_2O_3-SiO_2-H_2O (FMASH) system, as result of the following reactions (Vidal et al. 1992): 1) kaolinite + chlorite = carpholite + quartz + H_2O, 2) pyrophyllite + chlorite + H_2O = carpholite + quartz or in the

K_2O-FeO-MgO-Al_2O_3-SiO_2-H_2O (KFMASH) system (Oberhänsli et al. 1995; Bousquet et al. 2008), deriving from the reaction: 3) muscovite + chlorite + quartz + H_2O = celadonite + carpholite.

In the present study, the high temperature behavior of the Fe-carpholite from the quartz-calcite veins of the Pollino metapelites allowed to better understand the structure modification of this phase and its dissociation mechanism. A two step reaction scheme for the Fe-, Mg-carpholite dissociation was found instead of a three step reaction previously found in literature (Aoki 1966). It is to be noted that the reactions here proposed (as well as those reported by Aoki 1966) are expected to imply a significant change in the physicochemical conditions, specifically a strong change in O_2 fugacity. Likely, this is consequence of laboratory experiments carried out in air both *in situ* (present study) and *ex situ* (Aoki 1966). More work has to be performed with measurements under Ar or N_2 flux to avoid changes in O_2 fugacity, to check if this may produce a different assemblage for the carpholite decomposition. In any case, since there are no data about the thermal stability of the most widespread carpholite composition (iron-rich members) obtained by *in situ* analysis, our data contribute to understand the thermal evolution of H*P*/L*T* metasediments in collisional contexts. At the same time, the crystal chemical details obtained from a complete RT crystal structural analysis, including chemical occupancies of octahedral sites, may be of help for thermodynamic modelling of such complex carpholite-bearing systems. Future developments from *in situ* HT single crystal X-ray diffraction studies may also contribute to shed light on the potential of the deprotonated carpholite as a geothermometer as well as to detail the conditions and rate at which water (stored as OH^- in this phase) is released.

ACKNOWLEDGMENTS

The XRPD laboratory at the Dipartimento di Scienze della Terra and Geoambientali, University of Bari "Aldo Moro", was funded by Potenziamento Strutturale PONa3_00369 "Laboratorio per lo

Sviluppo Integrato delle Scienze e delle Tecnologie dei Materiali Avanzati e per dispositivi innovativi (SISTEMA)". The University of Basilicata contribution was supported by a G. Mongelli grant (RIL2016). Fernando Càmara and an anonymous referee are acknowledged for the attentive and insightful review of the manuscript.

REFERENCES CITED

Agard, P., Jolivet, L., and Goffé, B. (2001) Tectonometamorphic evolution of the Schistes Lustres Complex; implications for the exhumation of HP and UHP rocks in the Western Alps. Bulletin de la Société Géologique de France, 172(5), 617-636.

Agard, P., Labrousse, L., Elvevold, S., and Lepvrier, C. (2005) Discovery of Paleozoic Fe-Mg carpholite in Motalafjella, Svalbard Caledonides: A milestone for subduction-zone gradients. Geology, 33(10), 761-764.

Aoki, Y. (1966) Thermal reaction of carpholite. Mineralogical Journal, 5(1), 12-20.

Basso, R. and Carbone, C. (2010) Relationships between crystal data and crystal chemistry of carpholite-group minerals. Periodico di Mineralogia, 79(2), 91-98.

Basso, R., Cabella, R., Lucchetti, G., Martinelli, A., and Palenzona, A. (2005) Vanadiocarpholite, $Mn^{2+}V^{3+}Al(Si_2O_6)(OH)_4$, a new mineral from the Molinello mine, northern Apennines, Italy. European Journal of Mineralogy, 17, 501-507.

Bertoldi, C., Dachs, E., and Theye, T. (2006) Calorimetric data for naturally occurring magnesiocarpholite and ferrocarpholite. American Mineralogist, 91, 441-445.

Betteridge, P.W., Carruthers, J.R., Cooper, R.I., Prout, K., and Watkin, D.J. (2003) Crystals version 12: software for guided crystal structure analysis. Journal of Applied Crystallography, 36, 1487.

Bonardi, G., Amore, F.O., Ciampo, G., De Capoa, P., Miconnet, P., and Perrone, V. (1988) Il complesso Liguride. Auct.: stato delle conoscenze e problemi aperti sulla sua evoluzione pre-appenninica ed i suoi rapporti con l'arco calabro. Memorie Società Geologica Italiana, 41, 17-35.

Booth-Rea, G., Azanón, J.M., Goffé, G., Vidal, O., and Martínez-Martínez, J.M. (2002) High-pressure, low-temperature metamorphism in Alpujarride Units of southeastern Betics (Spain). Comptes Rendus Geosciences, 334(11), 857-865.

Bousquet, R., Oberhänsli, R., Goffe, B., Jolivet, L., and Vidal, O. (1998) High-pressure-low-temperature metamorphism and deformation in the Bündnerschiefer of the Engadine window: implications for the regional evolution of the eastern Central Alps. Journal of Metamorphic Geology, 16(5), 657-674.

Bousquet, R., Oberhänsli, R., Goffé, B., Wiederkehr, M., Koller, F., Schmid, S.M., Schuster, R., Engi, M., Berger, A., and Martinotti, G. (2008) Metamorphism of metasediments at the scale of an orogen: A key to the Tertiary geodynamic evolution of the Alps. In S. Siegesmund, B. Fügenschuh, N. Froitzheim, Eds., Tectonic Aspects of the Alpine-Dinaride-Carpathian System. Geological Society London Special Publications, 298, p. 393-411. The Geological Society of London 2008.

Brogi, A., and Giorgetti, G. (2012) Tectono-metamorphic evolution of the siliciclastic units in the Middle Tuscan Range (inner Northern Apennines): Mg-carpholite bearing quartz veins related to syn-metamorphic syn-orogenic foliation. Tectonophysics, 526-529, 167-184.

Brown, I.D. (2002) Topology and chemistry. Structural Chemistry, 13, 339-355.

Brown, I.D. and Altermatt, D. (1985) Bond-valence parameters obtained from a systematic analysis of the inorganic crystal structure database. Acta Crystallographica, B41, 244-247.

Bruker (2007) SAINT, Bruker AXS Inc., Madison, Wisconsin, USA.

Bruker (2009) SADABS, Bruker AXS Inc., Madison, Wisconsin, USA.

Bruker (2010) APEX2 v.2010.7-0, Bruker AXS Inc., Madison, Wisconsin, USA.

Busato, S. and Giampaolo, C. (1983) Ferrocarpholite from Mormanno (Northern Calabria, Italy). Periodico di Mineralogia, 52, 403-426.

Candan, O., Çetinkaplan, M., Oberhänsli, R., Rimmelé, G., and Akal, C. (2005) Alpine high-P/low-T metamorphism of the Afyon Zone and implications for the metamorphic evolution of Western Anatolia, Turkey. Lithos, 84(1-2), 102-124.

Cavalcante, F., Belviso, C., Finizio, F., Lettino, A., and Fiore, S. (2009). Carta geologica delle Unità Liguridi dell'area del Pollino (Basilicata): nuovi dati geologici, mineralogici e petrografici, 36 p. Regione Basilicata - Dip. Ambiente, Territorio e Politiche della Sostenibilità.

Cello, G., and Mazzoli, S. (1998) Apennine tectonics in southern Italy: a review. Journal of Geodynamics, 27, 191-211.

Dichicco, M.C., Laurita, S., Paternoster, M., Rizzo, G., Sinisi, R., and Mongelli, G. (2015) Serpentinite Carbonation for CO_2 Sequestration in the Southern Apennines: Preliminary Study. Energy Procedia, 76, 477-486.

Dichicco, M.C., De Bonis, A., Mongelli, G., Rizzo, G., and Sinisi, R. (2017) μ-Raman spectroscopy and X-ray diffraction of asbestos' minerals for geo-environmental monitoring: The case of the southern Apennines natural sources. Applied Clay Science, 141, 292-299.

Dichicco, M.C., Castiñeiras, P., Galindo Francisco, C., González Acebrón, L., Grassa, F., Laurita, S., Paternoster, M., Rizzo, G., Sinisi, R., and Mongelli, G. (2018) Genesis of carbonate-rich veins in the serpentinites at the Calabria-Lucania boundary (southern Apennines). Rendiconti Online della Società Geologica Italiana, 44, 143-149.

Escuder-Viruete, J., Pérez-Estaún, A., Booth-Rea, G., and Valverde-Vaquero, P. (2011) Tectonometamorphic evolution of the Samaná complex, northern Hispaniola: Implications for the burial and exhumation of high-pressure rocks in a collisional accretionary wedge. Lithos, 125, 190-210.

Ferraris, G., Ivaldi, G., and Goffé, B. (1992) Structural study of a magnesian ferrocarpholite: Are carpholites monoclinic?. Neues Jahrbuch für Mineralogie Monatshefte, 8, 337-347.

Fuchs, Y., Mellini, M., and Memmi, I. (2001) Crystal-chemistry of magnesiocarpholite: controversial X-ray diffraction, Mössbauer, FTIR and Raman results. European Journal of Mineralogy, 13, 533-543.

Ghose, S., Sen Gupta, P.K., Boggs, R.C., and Schlemper, E.O. (1989) Crystal chemistry of a nonstoichiometric carpholite, $K_x(Mn_{2-x}Li_x)Al_4Si_4O_{12}(OH)_4F_4$: A chain silicate related to pyroxenes. American Mineralogist, 74, 1084-1090.

Giorgetti, G., Goffé, B., Memmi, I., and Nieto, F. (1998) Metamorphic evolution of Verrucano metasediments in northern Apennines: new petrological constraints. European Journal of Mineralogy, 10, 1295-1308.

Goffé, B. (1980) Magnésiocarpholite, cookéite et euclase dans les niveaux continentaux métamorphiques de la zone briançonnaise. Données minéralogiques et nouvelles occurrences. Bulletin de Minéralogie, 103, 297-302.

Goffé, B., Michard, A., Kienast, J.R., and Le Mer, O. (1988) A case of obduction-related high-pressure, low-temperature metamorphism in upper crustal nappes, Arabian continental margin, Oman: P-T paths and kinematic interpretation. Tectonophysics, 151(1-4), 363-386.

Goffé, B. and Oberhänsli, R. (1992) Ferro- and magnesiocarpholite in the "Bündnerschiefer" of the eastern Central Alps (Grisons and Engadine Window). European Journal of Mineralogy, 4, 835-838.

Knott, S.D. (1987) The Liguride Complex of Southern Italy- a Cretaceous to Paleogene accretionary wedge. Tectonophysics, 142, 217-226.

Knott, S.D. (1994) Structure, kinematics and metamorphism in the Liguride Complex, southern Apennines, Italy. Journal of Structural Geology, 16, 1107-1120.

Kusiorowski, R., Zaremba, T., Gerle, A., Piotrowski, J., Simka, W., and Adamek, J. (2015) Study on the thermal decomposition of crocidolite asbestos. Journal of Thermal Analysis and Calorimetry, 120(3), 1585-1595.

Laurita, S. (2009). Il prisma di accrezione Liguride affiorante al confine Calabro-Lucano: Studio termocronologico e strutturale, 225 p. Ph.D. thesis, Università degli Studi della Basilicata, Potenza, Italy.

Laurita, S., and Rizzo, G. (2018) Blueschist metamorphism of metabasite dykes in the serpentinites of the Frido Unit, Pollino Massif. Rendiconti Online della Società Geologica Italiana, 45, 129-135.

Laurita, S., Prosser, G., Rizzo, G., Langone, A., Tiepolo, M., and Laurita, A. (2014) Geochronological study of zircons from continental crust rocks in the Frido Unit (Southern Apennines). International Journal of Earth Sciences (Geologische Rundschau), 104, 179-203.

Lindemann, W., Wögerbauer, R., and Berger P. (1979) Die kristallstruktur von karpholith $(Mn_{0.97}Mg_{0.08}Fe^{II}_{0.07})(Al_{1.90}Fe^{III}_{0.01})Si_2O_6(OH)_4$. Neues Jahrbuch für Mineralogie Monatshefte, 6, 282-287.

MacGillavry, C.H., Korst, W.L., Weichel Moore, E.J., and Van Der Plas, H.J. (1956) The crystal structure of ferrocarpholite. Acta Crystallographica, 9, 773-776.

Makreski, P., Jovanovski, G., Gajović, A., Biljan, T., Angelovski, D., and Jaćimović, R. (2006) Minerals from Macedonia. XVI. Vibrational spectra of some common appearing pyroxenes and pyroxenoids. Journal of Molecular Structure, 788, 102-114.

Monaco, C., Tortrici, L., Morten, L., Critelli, S., and Tansi, C. (1995) Geologia del versante nord-orientale del massiccio del Pollino (confine calabro-lucano): nota illustrativa sintetica della carta geologica alla scala 1:50000. Bollettino della Società Geologica Italiana, 114, 277-291.

Mottana, A., and Schreyer, W. (1977) Carpholite crystal chemistry and preliminary experimental stability. Neues Jahrbuch für Mineralogie Abhandlungen, 129(2), 113-138.

Naumova, I.S., Pobedimskaya, E.A., and Belov, N.V. (1974) Crystal structure of carpholite $MnAl_2(Si_2O_6)(OH)_4$. Kristallografiya, 19, 1155-1160.

Oberhänsli, R., Goffé, B., and Bousquet, R. (1995) Record of a HP–LT metamorphic evolution in the valais zone: Geodynamic implications. In B. Lombardo, Ed., Studies on metamorphic rocks and minerals of the western Alps. A volume in memory of Ugo Pognante, 13, p. 221-239. Bollettino del Museo Regionale di Scienze Naturali, Torino.

Oberhänsli, R., Partzsch, J., Candan, O., and Cetinkaplan, M. (2001) First occurrence of Fe-Mg-carpholite documenting a high-pressure metamorphism in metasediments of the Lycian Nappes, SW Turkey. International Journal of Earth Sciences, 89(4), 867-873.

Oberhänsli, R., Koralay, O.E., Candan, O., Pourteau, A., and Bousquet, R. (2013) Late Cretaceous eclogitic high-pressure relics in the Bitlis Massif. Geodinamica Acta, 26(3-4), 175-190.

Oberti, R., Boiocchi, M., Zema, M., Hawthorne, F.C., Redhammer, G.J., Susta, U., and Della Ventura, G. (2018) The high-temperature behaviour of riebeckite: expansivity, deprotonation, selective Fe oxidation and a novel cation disordering scheme for amphiboles. European Journal of Mineralogy, 30(3), 437- 449.

Palatinus, L., and Chapuis, G. (2007) Superflip - a computer program for the solution of crystal structures by charge flipping in arbitrary dimensions. Journal of Applied Crystallography, 40, 786-790.

Patacca, E., and Scandone, P. (2007) Geology of the Southern Apennines. Bollettino della Società Geologica Italiana, 7, 75-119.

Peng, Z., Ma, Z., and Han, S. (1987) The refinement of crystal structure of balipholite. Scientia Sinica, 30, 779-784.

Plunder, A., Agard, P., Dubacq, B., Chopin, C., and Bellanger, M. (2012) How continuous and precise is the record of P–T paths? Insights from combined thermobarometry and thermodynamic modelling into subduction dynamics (Schistes Lustrés, W. Alps). Journal of Metamorphic Geology, 30(3), 323-346.

Pourteau, A., Bousquet, R., Vidal, O., Plunder, A., Duesterhoeft, E., Candan, O., and Oberhänsli, R. (2014) Multistage growth of Fe-Mg-carpholite and Fe-Mg-chloritoid, from field evidence to thermodynamic modelling. Contribution to Mineralogy and Petrology, 168, 1090.

Renner, B., and Lehmann, G. (1986) Correlation of angular and bond length distortions in TO_4 units in crystals. Zeitschrift für Kristallographie, 175, 43-59.

Rimmelé, G., Oberhänsli, R., Goffé, B., Jolivet, L., Candan, O., and Cetinkaplan, M. (2003) First evidence of high-pressure metamorphism in the 'Civer Series' of the southern Menderes Massif. Tectonic and metamorphic implications for the evolution of SW Turkey. Lithos, 71, 19-46.

Rimmelé, G., Parra, T., Goffé, B., Oberhänsli, R., Jolivet, L., and Candan, O. (2005) Exhumation paths of high-pressure-low-temperature metamorphic rocks from the Lycian Nappes and the Menderes Massif (SW Turkey): a multi-equilibrium approach. Journal of Petrology, 46(3), 641-669.

Rimmelé, G., Oberhänsli, R., Candan, O., Goffé B., and Jolivet, L. (2006) The wide distribution of HP-LT rocks in the Lycian Belt (Western Turkey): implications for accretionary wedge geometry. In A.H.F. Robertson and D. Mountrakis, Eds., Tectonic Development of the Eastern Mediterranean Region, 260, p. 447-466. Geological Society, London, Special Publications.

Rizzo, G., Sansone, M.T.C, Perri, F., and Laurita, S. (2016) Mineralogy and petrology of the metasedimentary rocks from the Frido Unit (southern Apennines, Italy). Periodico di Mineralogia, 85(2), 153-168.

Rizzo, G., Laurita, S., and Altenberger, U. (2018) The Timpa delle Murge ophiolitic gabbros, southern Apennines: insights from petrology and geochemistry and consequences to the geodynamic setting. Periodico di Mineralogia, 87, 5-20.

Rizzo, G., Canora, F., Dichicco, M.C., Laurita, S., and Sansone, M.T.C. (2019) P-T estimates from amphibole and plagioclase pairs in metadolerite dykes of the Frido unit (southern Apennines-Italy) during the ocean-floor metamorphism. Journal of Mediterranean Earth Sciences, 11, doi: 10.3304/JMES.2019.003, in press.

Rossetti, F., Faccenna, C., Jolivet, L., Funiciello, R., Tecce, F., and Brunet, C. (1999) Syn- versus post-orogenic extension: the case study of Giglio Island (Northern Tyrrhenian Sea, Italy). Tectonophysics, 304, 71-93.

Rossetti, F., Faccenna, C., Goffé, B., Monié, P., Argentieri, A., Funiciello, R., and Mattei, M. (2001) Alpine structural and metamorphic signature of the Sila Piccola Massif nappe stack (Calabria, Italy): Insights for the tectonic evolution of the Calabrian Arc. Tectonics, 20, 112-133.

Rossetti, F., Goffé, B., Monié, P., Faccenna, C., and Vignaroli, G. (2004) Alpine orogenic P–T–t deformation history of the Catena Costiera area and surrounding regions (Calabrian Arc, southern

Italy): The nappe edifice of Northern Calabria revised with insights on the Tyrrhenian-Apennine system formation. Tectonics, 23, TC6011.

Sansone, M.T.C., Rizzo, G., and Mongelli, G. (2011) Petrochemical characterization of mafic rocks from the Ligurian ophiolites, southern Apennines. International Geology Review, 53, 130-156.

Sansone, M.T.C. and Rizzo, G. (2012) Pumpellyite veins in the metadolerite of the Frido Unit (southern Appennines-Italy). Periodico di Mineralogia, 81, 75-92.

Sansone, M.T.C., Prosser, G., Rizzo, G., and Tartarotti, P. (2012a) Spinel-peridotites of the Frido Unit ophiolites (Southern Apennines-Italy): evidence for oceanic evolution. Periodico di Mineralogia, 81(1), 35-59.

Sansone, M.T.C., Tartarotti, P., Prosser, G., and Rizzo, G. (2012b) From ocean to subduction: The polyphase metamorphic evolution of the Frido Unit metadolerite dykes (Southern Apennine, Italy). In G. Gosso, M. Iole Spalla, M. Zucali, Eds., Multiscale structural analysis devoted to the reconstruction of tectonic trajectories in active margins, 41, 3. Journal of the Virtual Explorer.

Sheldrick, G.M. (2008) XPREP, version 2008/2. Bruker-AXS, Madison, Wisconsin, USA.

Siivola, J. and Schmid, R. (2007) List of Mineral Abbreviations. Recommendations by the IUGS Subcommission on the Systematics of Metamorphic Rocks: Web version 01.02.2007 www.bgs.ac.uk/scmr/home.html.

Song, S.G., Zhang, L.F., Niu, Y., Wei, C.J., Liou, J.G., and Shu, G.M. (2007) Eclogite and carpholite-bearing metasedimentary rocks in the North Qilian suture zone, NW China: implications for Early Palaeozoic cold oceanic subduction and water transport into mantle. Journal of Metamorphic Geology, 25(5), 547-563.

Spadea, P. (1979) Contributo alla conoscenza dei metabasalti ofiolitici della Calabria settentrionale e centrale e dell'Appennino lucano. Rendiconti della Società Italiana di Mineralogia e Petrologia, 35(1), 251-276.

Spadea, P. (1982) Continental crust rocks associated with ophiolites in Lucanian Apennine (Southern Italy). Ofioliti, 7, 501-522.

Steen, D. and Bertrand, J. (1977) Sur la présence de ferrocarpholite associée aux schistes à glaucophane de Haute-Ubaye (Basses-Alpes, France). Schweizerische Mineralogische und Petrographische Mitteilungen, 57, 157-168.

Tait, K.T., Hawthorne, F.C., Grice, J.D., Jambor, J.L., and Pinchw, W.W. (2004) Potassic-carpholite, a new mineral species from the Sawtooth batholith, Boise County, Idhao, U.S.A. Canadian Mineralogist, 42, 121-124.

Theye, T., Seidel, E., and Vidal, O. (1992) Carpholite, sudoite, and chloritoid in low-grade high-pressure metapelites from Crete and the Peloponnese, Greece. European Journal of Mineralogy, 4, 487-507.

Theye, T., Reinhardt, J., Goffé, B., Jolivet, L., and Brunet, C. (1997). Ferro-and magnesiocarpholite from the Monte Argentario (Italy): First evidence for high-pressure metamorphism of the metasedimentary Verrucano sequence, and significance for P-T path reconstruction. European Journal of Mineralogy, 9, 859-873.

Toby, B. H., and Von Dreele, R. B. (2013). GSAS-II: the genesis of a modern open-source all purpose crystallography software package. Journal of Applied Crystallography, 46(2), 544-549.

Tortorici, L., Catalano, S., and Monaco, C. (2009) Ophiolite-bearing mélanges in southern Italy. Geological Journal, 44(2), 153-166.

Trotet, F., Goffé, B., Vidal, O., and Jolivet, L. (2006) Evidence of retrograde Mg-carpholite in the Phyllite-Quartzite nappe of Peloponnese from thermobarometric modelisation-geodynamic implications. Geodynamica Acta, 19(5), 323-343.

Ventruti, G., Zema, M., Scordari, F., and Pedrazzi, G. (2008) Thermal behavior of a Ti-rich phlogopite from Mt. Vulture (Potenza, Italy): An in situ X-ray single-crystal diffraction study. American Mineralogist, 93, 632-643.

Verlaguet, A., Goffé, B., Brunet, F., Poinssot, C., Vidal, O., Findling, N., and Menut, D. (2011) Metamorphic veining and mass transfer in a chemically closed system: a case study in Alpine metabauxites (western Vanoise). Journal of Metamorphic Geology, 29(3), 275-300.

Vidal, O., Goffé, B., and Theye, T. (1992) Experimental study of the stability of sudoite and magnesiocarpholite and calculation of a new petrogenetic grid for the system FeO–MgO–Al_2O_3–SiO_2–H_2O. Journal of Metamorphic Geology, 10, 603-614.

Viswanathan, K. (1981) The crystal structure of a Mg-rich carpholite. American Mineralogist, 66, 1080-1085.

Viswanathan, K. and Seidel, E. (1979) Crystal chemistry of Fe-Mg-carpholites. Contribution to Mineralogy and Petrology, 70, 41- 47.

Vitale, S., Fedele, L., D'Assisi Tramparulo, F., Ciarcia, S., Mazzoli, S., and Novellino, A. (2013) Structural and petrological analyses of the Frido Unit (southern Italy): New insights into the early tectonic evolution of the southern Apennines-Calabrian Arc system. Lithos, 168-169, 219-235.

Welch, M.D., Mitchell, R.H., Kampf, A.R., Chakhmouradian, A.R., Smith, D., and Carter, M. (2014) Crystal structure and topological affinities of magbasite, $KBaFe^{3+}Mg_7Si_8O_{22}(OH)_2F_6$: a trellis structure related to amphibole and carpholite. Mineralogical Magazine, 78(1), 29-45.

Zema, M., Ventruti, G., Lacalamita, M., and Scordari, F. (2010) Kinetics of Fe-oxidation/deprotonation process in Fe-rich phlogopite under isothermal conditions. American Mineralogist, 95, 1458-1466.

Figure captions

Figure 1. Sketch of the southern Apennines (A); Geological map of the northeastern area of the Pollino Massif (B) indicating the sampling site (C); (D) a detail of (C**)** showing hand-sample carpholite.

Figure 2. Microphotographs of carpholite needles embedded in quartz (A, B, cross polarized, 10X); SEM images showing aggregates of carpholite crystals and the relative EDS spectrum (C, D); back scattered electron images of carpholite crystals embedded in microcrystalline quartz (E, F). Mineral abbreviations after Siivola and Schmidt (2007): Cph, carpholite; Qtz, quartz; Cal, calcite.

Figure 3. Mg-Mn-Fe ternary diagram showing the composition of the studied and literature carpholites (modified after Vitale et al. 2013). Symbols: Green solid squares indicate the craph4 crystals in this study. Blue triangles represent samples in Vitale et al. (2013). Black symbols for carpholites in literature where unit cell parameters or structure refinements are available (solid square: Mottana and Schreyer 1977; solid circle: Steen and Bertrand 1977; solid triangle pointing upward: Viswanathan and Seidel 1979; solid triangle pointing downward: Ferraris et al. 1992; solid diamond: Bertoldi et al. 2006; plus: Viswanathan 1981; cross: Fuchs et al. 2001; star: Goffé 1980; circle with horizontal line: Lindeman et al. 1979; triangle pointing upward with horizontal line: Basso et al. 2005; triangle pointing downward with horizontal line: Peng et al. 1987; diamond with horizontal line: Ghose et al. 1989; square with vertical line: Tait et al. 2004). Pink symbols for other literature carpholites (triangle pointing upward with vertical line: Agard et al. 2005; triangle pointing downward with vertical line: Pourteau et al. 2014; square with cross inside: Vidal et al.

1992; circle with cross inside: Brogi and Giorgetti 2012; triangle pointing upward with cross inside: Rossetti et al. 1999; triangle pointing downward with cross inside: Rossetti et al. 2001; square with plus inside: Rossetti et al. 2004; pentagon: Giorgetti et al. 1998).

Figure 4. Crystal **s**tructure of the Carph4_1 sample as seen along [001] (a). The O-O distances of the diagonals of the channels are reported. (b) M1-M3 ribbon projected along [100].

Figure 5. Relationship between the X_{Fe} and the values of the *a* (a), *b* (b) and *c* (c) cell parameters. The straight lines are guide to the eyes, and are traced excluding the carpholites in Mottana and Schreyer (1977), Lindemann et al. (1979), Basso et al. (2005), Ghose et al. (1989), Tait et al. (2004) and Peng et al. (1987). Symbols as in Figure 3.

Figure 6. Representative experimental (red line) µRaman spectra of the studied Fe-carpholite at low (a) and high frequency (b). In the low frequency region, the Raman shift data retrieved from the RRUFF Raman spectroscopy database (black line) is also shown for comparison.

Figure 7. Orientation of the OH groups in the studied Fe-carpholite.

Figure 8. TG (blue line), DTA (black line) and DTG (red line) curves of Fe-carpholite measured in air.

Figure 9. Selected XRPD patterns of carpholite showing the evolution of the diffraction data in the temperature range 30-605°C (a) and 630-1105°C (b). For the 30-605°C patterns, selected 2θ range are shown (see text). Labels: M = mullite; S = spinel; G = garnet (almandine); Cr = cristobalite; T = tridymite; Q = quartz.

Figure 10. Normalized volume and unit cell parameters of the studied carpholite versus temperature. a_0, b_0, c_0 and V_0 are lattice parameters and unit cell volume at room temperature, respectively. Symbols: solid for the Fe-carpholite phase; empty for the deprotonated Fe-carpholite phase. The size of the symbols is larger than the associated esd's.

This is the peer-reviewed, final accepted version for American Mineralogist, published by the Mineralogical Society of America.
The published version is subject to change. Cite as Authors (Year) Title. American Mineralogist, in press.
DOI: https://doi.org/10.2138/am-2020-7385. http://www.minsocam.org/

Table 1. Selected crystallographic data for the studied Fe-carpholite.

	Carph4_1	**Carph4_3**
Crystal size (mm^3)	0.60 × 0.13 × 0.05	0.20 × 0.08 × 0.04
Space group	*Ccce*	*Ccce*
***a* (Å)**	13.7656(4)	13.7687(8)
***b* (Å)**	20.1426(6)	20.168(1)
***c* (Å)**	5.1122(2)	5.1146(3)
Cell volume (Å^3)	1417.48(6)	1420.2(1)
Measured reflections	20690	9763
Independent reflections	2702	1737
$R_{merging}$ [$R_{(int)}$] (%)	2.6	5.6
h_{min}, h_{max}	-26, 27	-22, 21
k_{min}, k_{max}	-38, 36	-33, 21
l_{min}, l_{max}	-9, 9	-8, 7
Reflections used ($I > 3\sigma(I)$)	2116	1095
No. of refined parameters	71	71
Goof[a]	1.105	1.115
R[b] [on F] (%)	2.3	2.6
R_w[c] [on F^2] (%)	1.9	2.5
$\Delta\rho_{min}/\Delta\rho_{max}$ (e$^-$/Å^3)	-0.52/0.69	-0.48/41

[a]Goodness of fit = $[S[w(F_o^2-F_c^2)^2]/(N-p)]^{1/2}$, where N and p are the number of reflections and parameters, respectively.
[b]$R = S[|F_o| - |F_c|]/S|F_o|$. [c]$R_w = [S[w(F_o^2-F_c^2)^2]/S[w(F_o^2)^2]]^{1/2}$; w = Chebyshev optimized weights.

This is the peer-reviewed, final accepted version for American Mineralogist, published by the Mineralogical Society of America.
The published version is subject to change. Cite as Authors (Year) Title. American Mineralogist, in press.
DOI: https://doi.org/10.2138/am-2020-7385. http://www.minsocam.org/

Table 2. Crystallographic coordinates, occupancies, equivalent isotropic ($Å^2$) and anisotropic displacement parameters of the studied Fe-carpholite.

Sample Carph4_1

Site	Atom	*x*/*a*	*y*/*b*	*z*/*c*	Occupancy	$U_{iso/equiv}$	U_{11}	U_{22}	U_{33}	U_{12}	U_{13}	U_{23}
M1	Mg Fe	0	0.625627 (9)	0.75	0.372 (2) 0.628 (2)	0.0085	0.00837 (7)	0.00797 (7)	0.00902 (7)	0	-0.00130 (6)	0
M2 ≡ Al(1)	Al	0.19114(2)	0.75	0.75		0.0067	0.00779 (9)	0.0059 (1)	0.0065 (1)	0	0	0.0005 (1)
M3 ≡ Al(2)	Al	0	0.96123 (1)	0.25		0.0066	0.00728 (9)	0.0068 (1)	0.0056 (1)	0	-0.0002 (1)	0
Si	Si	0.19371(1)	0.879813(9)	0.41764(4)		0.0059	0.00646(6)	0.00580(6)	0.00557(6)	0.00057(5)	0.00007(5)	0.00029(6)
O(1)	O	0.20591(3)	0.79992(2)	0.4318(1)		0.0077	0.0095(2)	0.0060(2)	0.0078(2)	0.0008(1)	0.0007(2)	0.0005(1)
O(2)	O	0.08091(3)	0.89934(3)	0.4059(1)		0.0084	0.0070(2)	0.0097(2)	0.0086(2)	0.0017(1)	-0.0001(1)	0.0013(2)
O(3)	O	0.24730(4)	0.91260(2)	0.6730(1)		0.0087	0.0111(2)	0.0081(2)	0.0070(2)	-0.0001(2)	-0.0025(1)	0.0002(2)
O(4) ≡ OH(1)	O	0.10006(4)	0.80917(3)	0.8828(1)		0.0116	0.0119(2)	0.0129(2)	0.0100(2)	0.0038(2)	0.0004(2)	-0.0003(2)
O(5) ≡ OH(2)	O	0.06790(3)	0.96616(3)	0.9276(1)		0.0080	0.0071(2)	0.0092(2)	0.0078(2)	0.0012(1)	0.0006(1)	0.0005(2)
H(1)	H	0.0952	0.6984	0.4586		0.0208						
H(2)	H	0.1282	0.9622	0.9226		0.0161						

Sample Carph4_3

Site	Atom	*x*/*a*	*y*/*b*	*z*/*c*	Occupancy	$U_{iso/equiv}$	U_{11}	U_{22}	U_{33}	U_{12}	U_{13}	U_{23}
M1	Mg Fe	0	0.62558(2)	0.75	0.394(4) 0.606(4)	0.0072	0.0067(2)	0.0069(2)	0.0079(2)	0	-0.0014(2)	0
M2 ≡ Al(1)	Al	0.19103(5)	0.75	0.75		0.0057	0.0064(3)	0.0054(2)	0.0053(3)	0	0	0.0005(3)
M3 ≡ Al(2)	Al	0	0.96128(4)	0.25		0.0059	0.0061(2)	0.0067(3)	0.0048(3)	0	-0.0005(3)	0
Si	Si	0.19370(3)	0.87982(2)	0.4177(1)		0.0050	0.0053(2)	0.0055(2)	0.0043(2)	0.0008(2)	0.0001(2)	0.0001(2)
O(1)	O	0.20585(9)	0.79981(6)	0.4319(3)		0.0067	0.0085(5)	0.0048(4)	0.0068(5)	0.0006(4)	0.0008(4)	0.0008(4)
O(2)	O	0.08098(9)	0.89934(6)	0.4065(3)		0.0077	0.0057(4)	0.0094(5)	0.0081(5)	0.0019(4)	-0.0005(4)	0.0011(5)
O(3)	O	0.2474(1)	0.91266(6)	0.6727(3)		0.0075	0.0098(4)	0.0073(4)	0.0055(4)	0.0002(5)	-0.0027(4)	-0.0002(4)
O(4) ≡ OH(1)	O	0.1001(1)	0.80925(7)	0.8821(3)		0.0108	0.0105(5)	0.0136(5)	0.0085(5)	0.0037(4)	0.0005(4)	-0.0003(5)
O(5) ≡ OH(2)	O	0.06792(8)	0.96615(6)	0.9276(3)		0.0070	0.0052(4)	0.0088(4)	0.0069(5)	0.0006(4)	0.0010(4)	0.0009(4)
H(1)	H	0.0877	0.6981	0.4653		0.0175						
H(2)	H	0.1277	0.9619	0.9236		0.0108						

This is the peer-reviewed, final accepted version for American Mineralogist, published by the Mineralogical Society of America.
The published version is subject to change. Cite as Authors (Year) Title. American Mineralogist, in press.
DOI: https://doi.org/10.2138/am-2020-7385. http://www.minsocam.org/

Table 3. Selected geometrical parameters for the studied and literature carpholites. Bond distances are reported in Å.

	Ferrocarpholite			Magnesiocarpholite			Carpholite	Vanadiocarphonite		Potassic-carpholite
	This study		Ferraris et al. (1992)	Viswanathan (1981)	Fuchs at al. (2001)		Lindemann et al. (1979)	Basso et al. (2005)		Ghose et al. (1989)
	Carph4_1	Carph4_3			MA	ML		VrC	VC	
M1-OH(1) x2	2.0206(6)	2.021(1)	2.030(1)	2.009(2)	2.006(1)	2.005(1)	2.067(4)	2.067(4)	2.082(3)	2.107(2)
M1-O(2) x2	2.1419(5)	2.141(1)	2.156(1)	2.111(3)	2.122(1)	2.115(1)	2.183(4)	2.181(5)	2.169(3)	2.154(2)
M1-OH(2)x2	2.2620(5)	2.263(1)	2.273(1)	2.234(2)	2.242(1)	2.239(1)	2.312(4)	2.306(4)	2.271(3)	2.272(2)
<M1-O>	2.1415(3)	2.142(1)	2.15(4)	2.118(1)	2.123(1)	2.120	2.19(4)	2.185	2.174	2.178
M2-OH(1) x2	1.8582(6)	1.858(1)	1.855(1)	1.857(2)	1.855(1)	1.856(1)	1.830(4)	1.819(4)	1.827(3)	1.808(1)
M2-O(1) x2	1.9233(5)	1.923(1)	1.925(1)	1.920(2)	1.925(1)	1.923(1)	1.932(5)	1.975(5)	2.022(3)	1.914(1)
M2-O(1)' x2	1.9705(5)	1.973(1)	1.970(1)	1.963(2)	1.965(1)	1.961(1)	1.949(5)	2.033(4)	2.084(3)	1.928(1)
<M2-O>	1.9173(3)	1.918(1)	1.92(2)	1.913(1)	1.915(1)	1.913	1.90(2)	1.942	1.978	1.883
M3-O(2) x2	1.8519(5)	1.856(1)	1.858(1)	1.853(2)	1.851(1)	1.854(1)	1.855(4)	1.867(4)	1.894(3)	1.860(2)
M3-OH(2) x2	1.8973(5)	1.898(1)	1.899(1)	1.896(3)	1.897(1)	1.896(1)	1.890(4)	1.898(5)	1.934(3)	1.890(2)
M3-OH(2)' x2	1.9589(5)	1.960(1)	1.963(1)	1.961(2)	1.957(1)	1.962(1)	1.951(4)	1.973(4)	1.986(3)	1.955(2)
<M3-O>	1.9027(3)	1.905(1)	1.91(2)	1.903(1)	1.902(1)	1.904	1.90(2)	1.913	1.938	1.902
Si -O(2)	1.6030(5)	1.602(1)	1.601(1)	1.601(3)	1.600(1)	1.603(1)	1.589(4)	1.607(4)	1.605(3)	1.595(2)
Si-O(1)	1.6196(5)	1.624(1)	1.623(1)	1.619(3)	1.615(1)	1.618(1)	1.613(6)	1.633(4)	1.627(3)	1.630(2)
Si-O(3)	1.6310(6)	1.633(1)	1.362(1)	1.630(3)	1.631(1)	1.630(1)	1.622(5)	1.624(5)	1.630(3)	1.629(2)
Si-O(3)'	1.6383(6)	1.639(1)	1.643(1)	1.639(3)	1.637(1)	1.642(1)	1.635(5)	1.638(5)	1.645(3)	1.641(2)
<Si-O>	1.6230(3)	1.625(1)	1.625(8)	1.622(2)	1.621(1)	1.623	1.615(8)	1.6255	1.62675	1.624
O(4)-H(1)	0.828	0.809								
O(5)-H(2)	0.834	0.827								
K-OH(1) x4					2.628(1)	2.640(1)		2.623(5)	2.629(3)	2.674(4)
K-O(1) x4					3.137(1)	3.142(1)		3.144(4)	3.127(3)	3.153(4)
K-O(2) x4					3.297(1)	3.299(1)		3.361(4)	3.400(3)	3.294(4)
K-OH(1)' x4								3.749(5)	3.757(3)	3.648(4)
<K-O>					3.021(1)	3.027(1)		3.219(2)	3.228(2)	3.192(3)
BLD_{M1}	5.690	5.704	5.731	5.311	5.563	5.519	5.779	5.635	4.459	4.007
BLD_{M2}	2.658	2.696	2.739	2.513	2.625	2.506	3.041	5.217	6.322	3.093
BLD_{M3}	2.532	2.466	2.502	2.563	2.506	2.566	2.292	2.569	2.175	2.289
O(4)-O(4)*	3.629	3.648	3.644	3.642	3.640	3.649	3.655	3.672	3.635	3.617
L/S**	1.753	1.753	1.752	1.756	1.758	1.761	1.709	1.695	1.663	1.713

Notes: BLD: bond-length distortions (Renner and Lehmann 1986). *The O4-O4 represents the diagonal of the four-membered channel (see Figure 4); **L/S is the ratio of the longest (O2-O2 distance) and shortest (O3-O3 distance) diagonals of the eight-membered channel (see Figure 4).

This is the peer-reviewed, final accepted version for American Mineralogist, published by the Mineralogical Society of America.
The published version is subject to change. Cite as Authors (Year) Title. American Mineralogist, in press.
DOI: https://doi.org/10.2138/am-2020-7385. http://www.minsocam.org/

Table 4. Crystal chemical formulae (in atoms per formula unit, apfu) of the studied and refined carpholites in the literature.

Specimen	Sample	Chemical formula	Reference
Ferrocarpholite	Carph4_1	$(Fe^{2+}_{0.63}Mg_{0.37})Al_2Si_2O_6(OH)_4$	This study
	Carph4_3	$(Fe^{2+}_{0.61}Mg_{0.39})Al_2Si_2O_6(OH)_4$	This study
		$(Fe^{2+}_{0.76}Mg_{0.24})Al_2Si_2O_6(OH)_4$	Ferraris et al. (1992)
Magnesiocarpholite	MA	$K_{0.002}(Fe^{2+}_{0.32}Fe^{3+}_{0.03}Mg_{0.65})Al_{1.97}Si_{2.00}O_{5.90}(OH)_{3.95}F_{0.15}$	Fucks et al. (2001)
	ML	$K_{0.002}(Fe^{2+}_{0.34}Fe^{3+}_{0.01}Mg_{0.65})Al_{1.98}Si_{2.00}O_{5.92}(OH)_{3.96}F_{0.12}$	Fucks et al. (2001)
Carpholite		$(Mn_{0.97}Fe_{0.07}Mg_{0.08})(Al_{1.90}Fe^{3+}_{0.01})Si_{2.00}O_{6.00}(OH)_4$	Lindemann et al. (1979)
Vanadiocarphlnite	VrC	$K_{0.01}(Mn_{0.85}Fe_{0.02}Mg_{0.11})(Al_{1.52}V^{3+}_{0.51})Si_{1.99}O_6(OH)_{4.00}$	Basso et al. (2005)
	VC	$K_{0.07}(Mn_{0.90}Fe_{0.01}Mg_{0.09})(Al_{1.00}V^{3+}_{0.98})Si_{1.97}O_6(OH)_{4.11}$	Basso et al. (2005)
Potassic-carpholite		$K_{0.35}(Mn_{0.63}Fe_{0.03}Mg_{0.01}L_{i0.26}Na_{0.08})Al_{1.98}Si_{2.00}O_{5.88}(OH)_{2.53}F_{1.59}$	Ghose et al. (1989)

Table 5. Unit cell parameters of the studied Fe-carpholite as a function of T.

T (°C)	Phase	*a* (Å)	*b* (Å)	*c* (Å)	V (Å^3)
30	c	13.757(7)	20.141(8)	5.090(3)	1410(2)
55	c	13.760(7)	20.152(8)	5.092(3)	1411(2)
80	c	13.756(6)	20.157(8)	5.094(3)	1412(2)
105	c	13.756(7)	20.163(8)	5.097(3)	1414(2)
130	c	13.755(7)	20.169(8)	5.103(3)	1416(2)
155	c	13.751(7)	20.173(8)	5.103(3)	1416(2)
180	c	13.756(7)	20.187(8)	5.106(3)	1418(2)
205	c	13.752(7)	20.189(8)	5.108(3)	1418(2)
230	c	13.754(2)	20.200(8)	5.110(3)	1420(2)
255	c	13.752(7)	20.205(8)	5.114(3)	1421(2)
280	c	13.753(7)	20.213(8)	5.116(3)	1422(2)
305	c	13.754(7)	20.220(8)	5.114(3)	1422(2)
330	c	13.754(7)	20.228(8)	5.115(3)	1423(2)
355	c	13.743(6)	20.224(8)	5.114(3)	1422(2)
380	c	13.738(7)	20.229(8)	5.107(3)	1419(2)
	dc	13.98(3)	20.075(9)	4.30(5)	1205(2)
405	c	13.734(6)	20.231(7)	5.092(3)	1415(1)
	dc	13.66(1)	20.089(7)	4.811(2)	1320(2)
430	c	13.737(1)	20.245(7)	5.063(1)	1408(1)
	dc	13.658(7)	20.101(1)	4.802(1)	1318(1)
455	c	13.721(5)	20.237(7)	5.068(3)	1407(1)
	dc	13.665(6)	20.086(7)	4.805(2)	1319(1)
480	c	13.718(2)	20.245(7)	5.061(1)	1405(1)
	dc	13.671(2)	20.090(1)	4.813(1)	1322(1)
505	c	13.732(6)	20.264(7)	5.067(2)	1410(1)
	dc	13.692(6)	20.101(7)	4.797(2)	1320(1)
530	c	13.740(4)	20.266(1)	5.060(1)	1409(1)
	dc	13.713(2)	20.127(1)	4.808(1)	1327(1)
555	c	13.711(8)	20.241(9)	5.045(5)	1400(2)
	dc	13.716(7)	20.129(9)	4.812(3)	1329(2)
580	c	13.716(8)	20.207(8)	5.080(4)	1408(1)
	dc	13.713(7)	20.131(8)	4.807(3)	1327(2)
605	dc	13.761(7)	20.175(8)	5.039(2)	1399(1)
630	dc	13.77(3)	20.15(4)	4.92(2)	1365(9)

Note: c = Fe-carpholite; dc = deprotonated Fe-carpholite.

This is the peer-reviewed, final accepted version for American Mineralogist, published by the Mineralogical Society of America.
The published version is subject to change. Cite as Authors (Year) Title. American Mineralogist, in press.
DOI: https://doi.org/10.2138/am-2020-7385. http://www.minsocam.org/

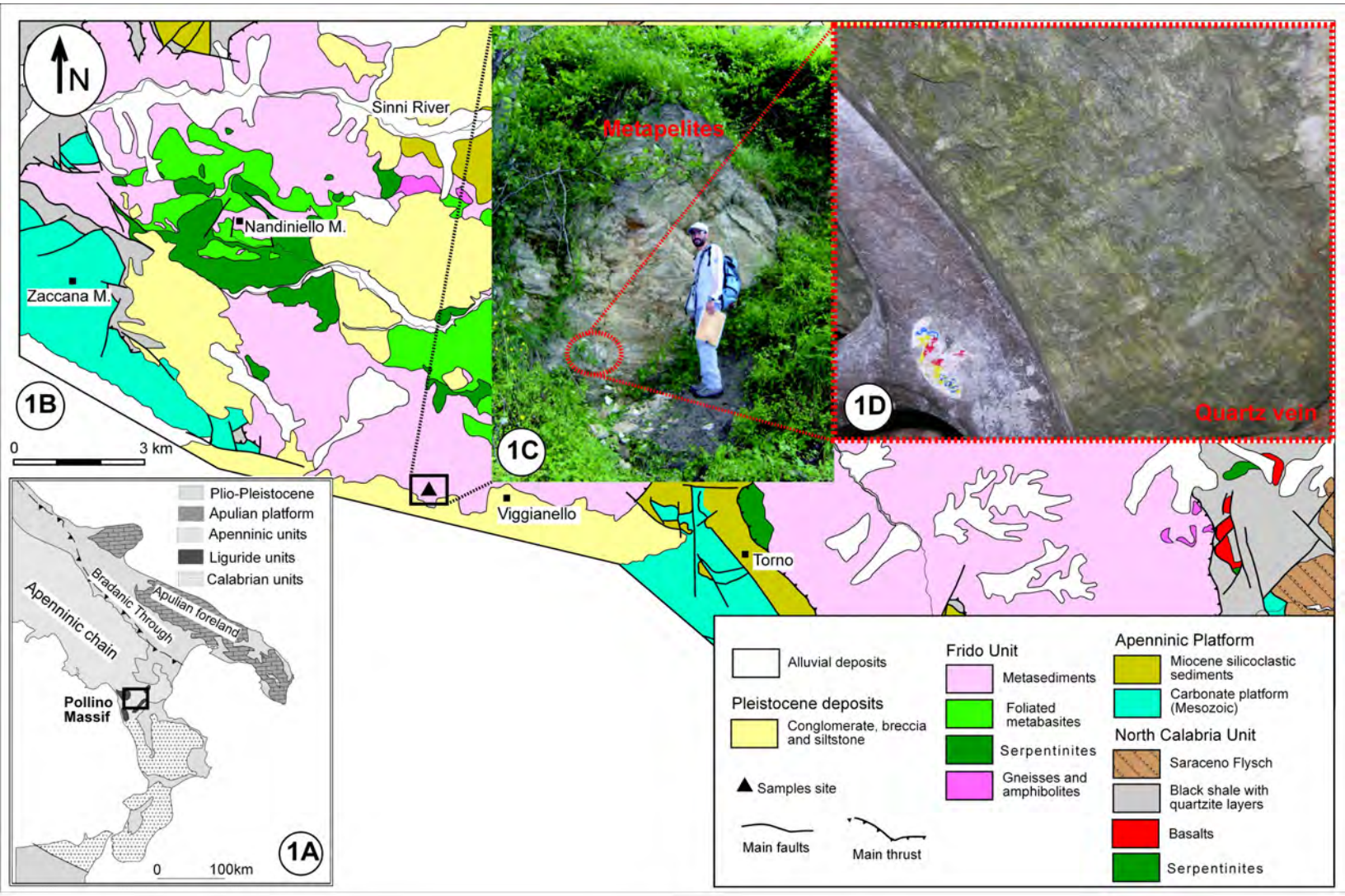

Fig 1

This is the peer-reviewed, final accepted version for American Mineralogist, published by the Mineralogical Society of America.
The published version is subject to change. Cite as Authors (Year) Title. American Mineralogist, in press.
DOI: https://doi.org/10.2138/am-2020-7385. http://www.minsocam.org/

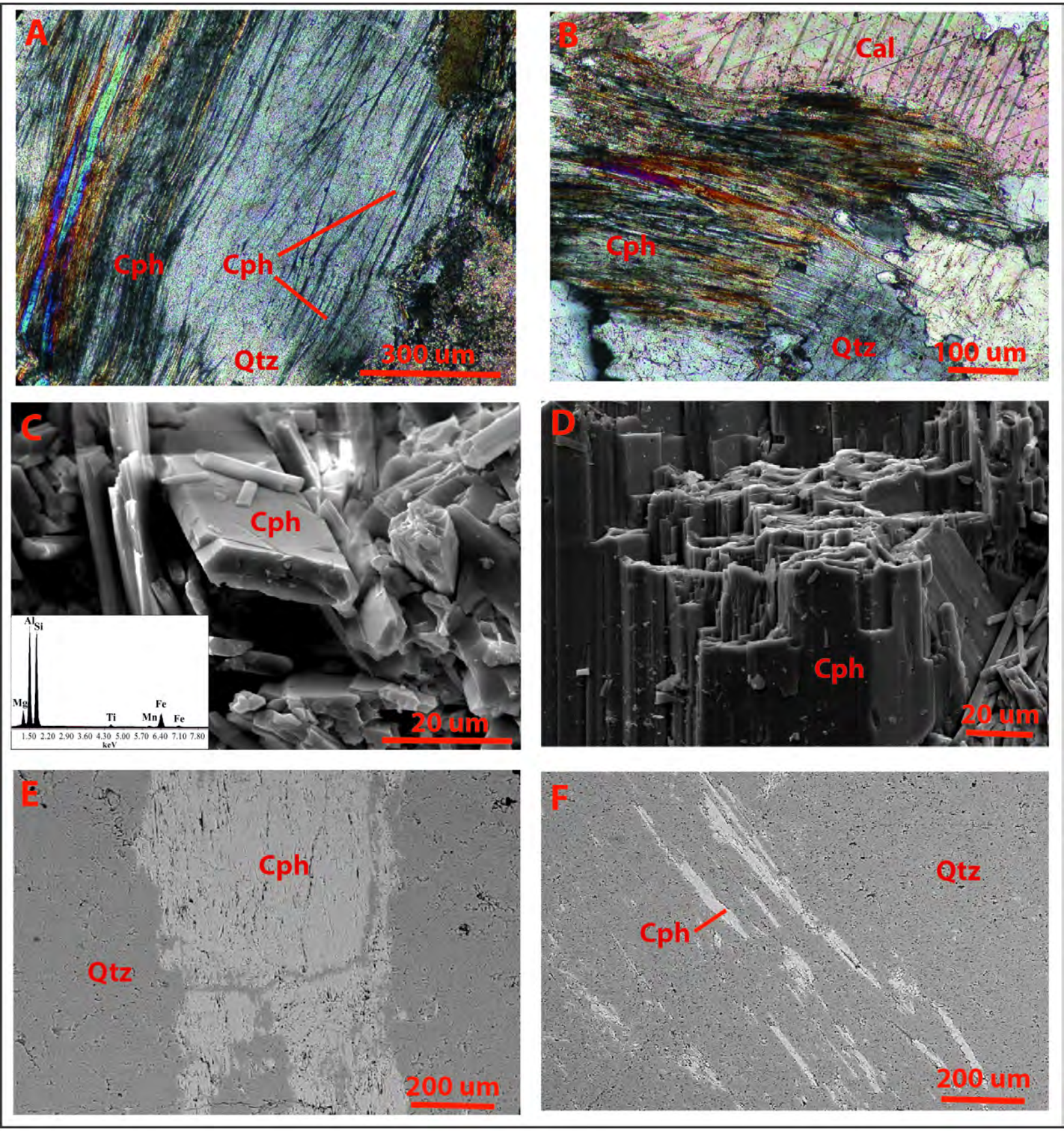

Fig 2

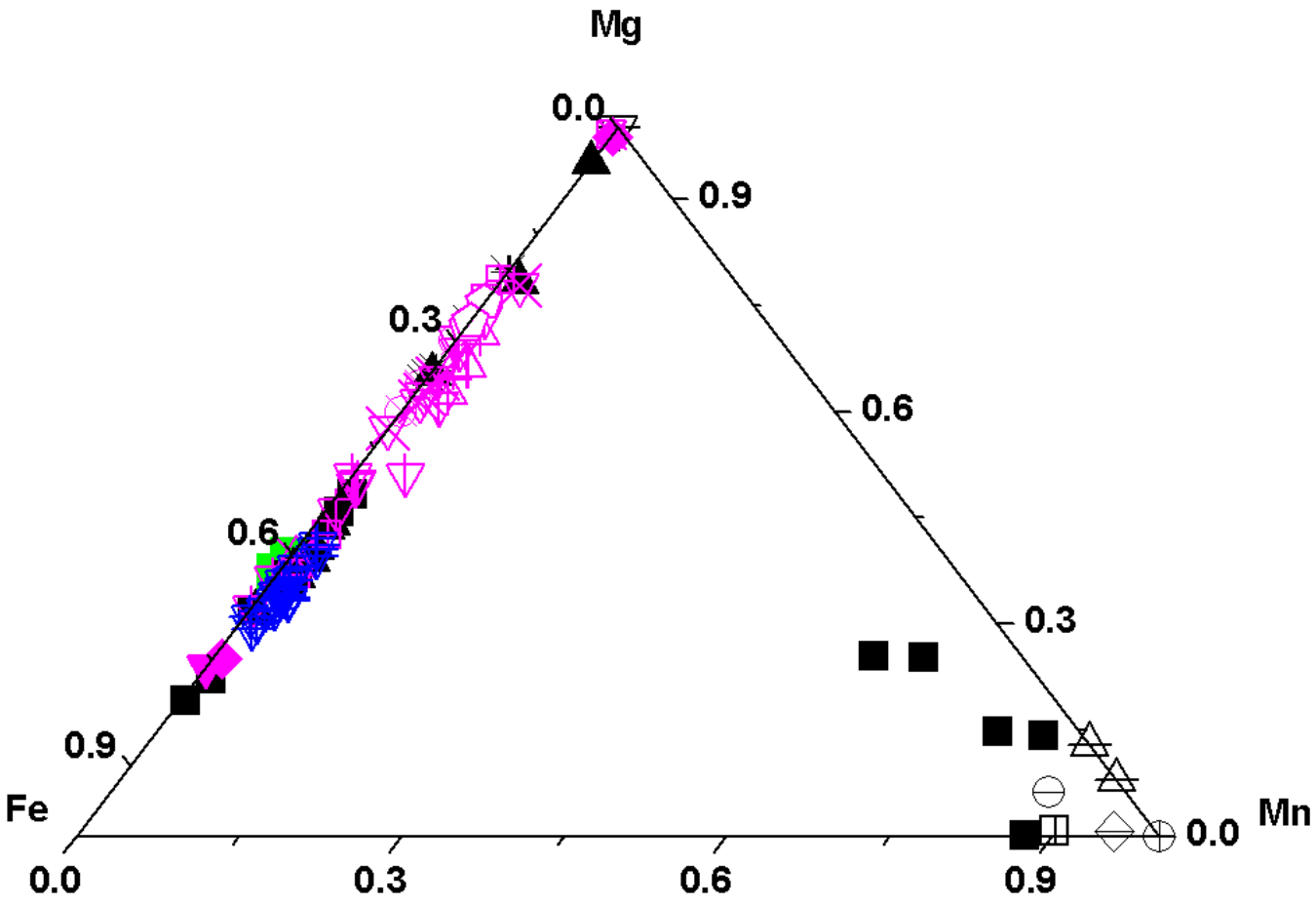

Fig 3

This is the peer-reviewed, final accepted version for American Mineralogist, published by the Mineralogical Society of America.
The published version is subject to change. Cite as Authors (Year) Title. American Mineralogist, in press.
DOI: https://doi.org/10.2138/am-2020-7385. http://www.minsocam.org/

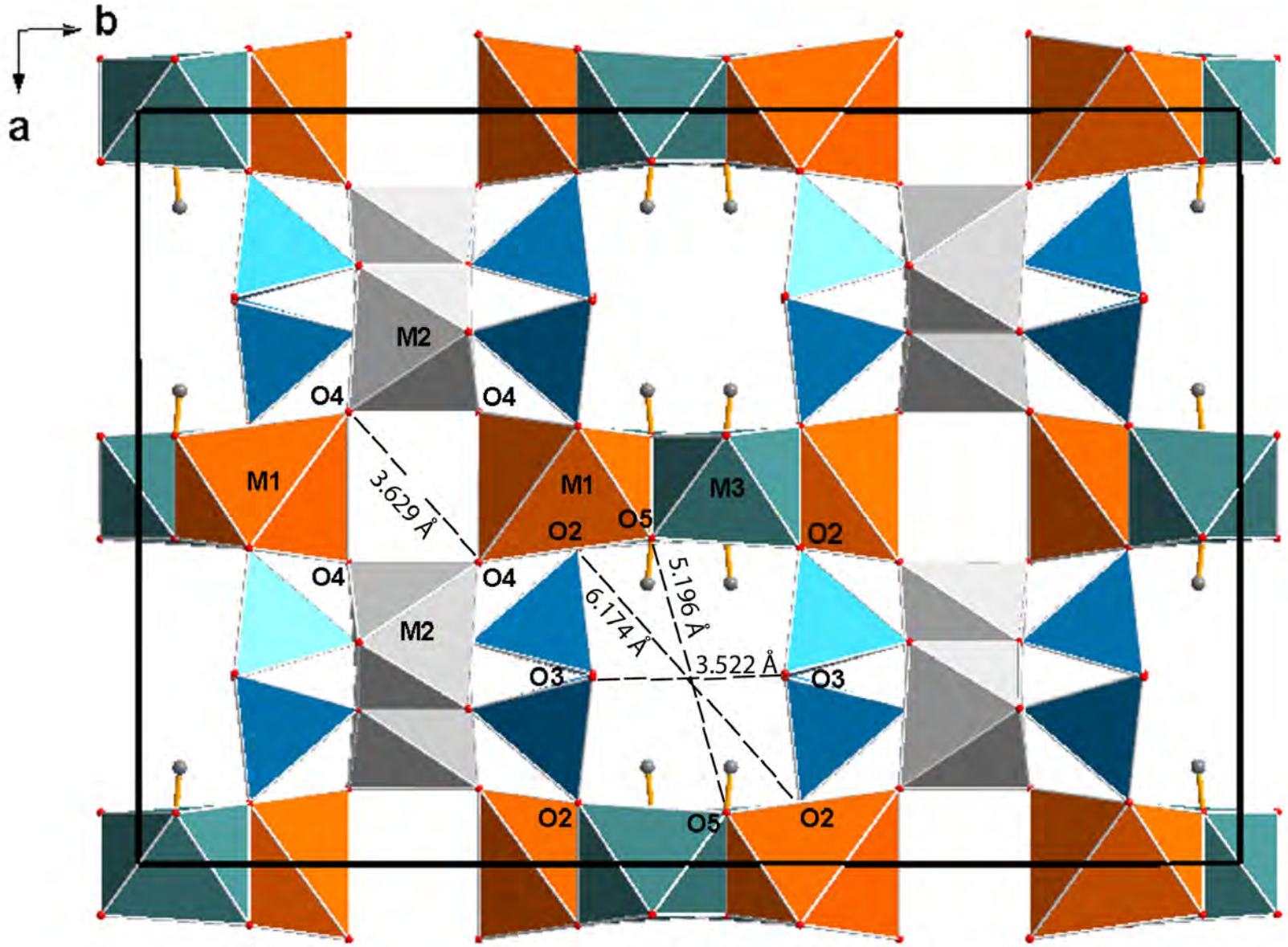

Fig 4a

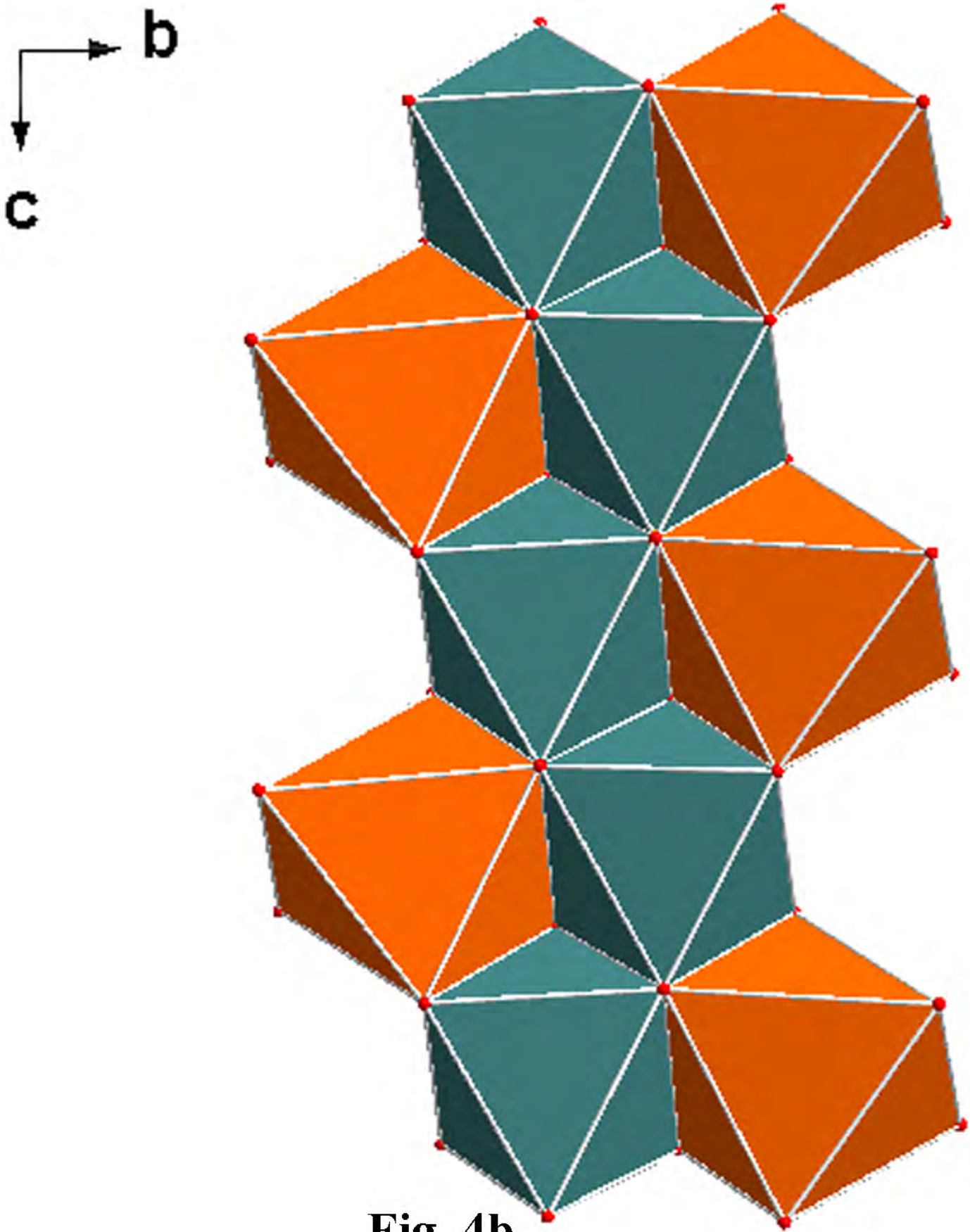

Fig. 4b

This is the peer-reviewed, final accepted version for American Mineralogist, published by the Mineralogical Society of America.
The published version is subject to change. Cite as Authors (Year) Title. American Mineralogist, in press.
DOI: https://doi.org/10.2138/am-2020-7385. http://www.minsocam.org/

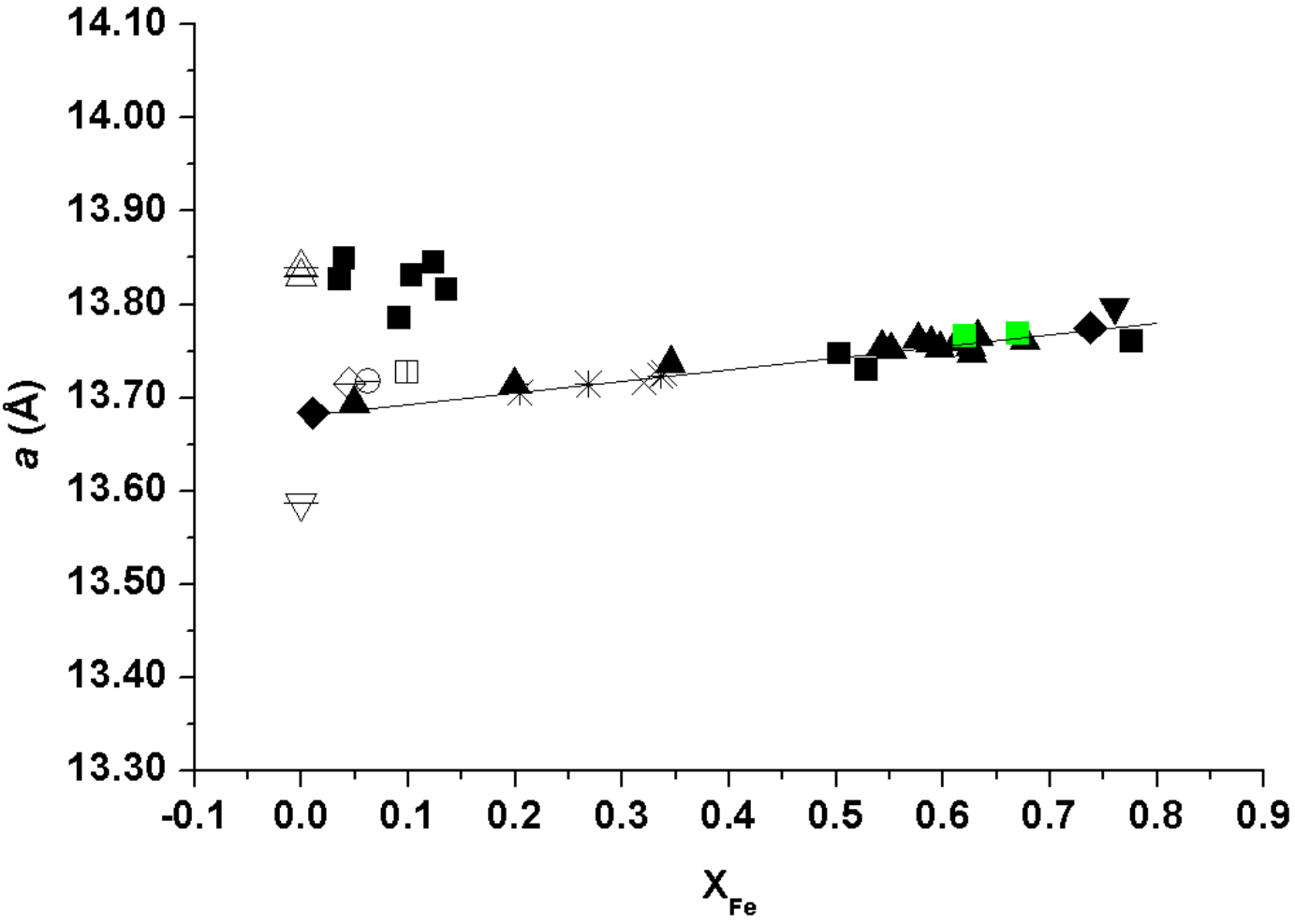

Fig 5a

This is the peer-reviewed, final accepted version for American Mineralogist, published by the Mineralogical Society of America.
The published version is subject to change. Cite as Authors (Year) Title. American Mineralogist, in press.
DOI: https://doi.org/10.2138/am-2020-7385. http://www.minsocam.org/

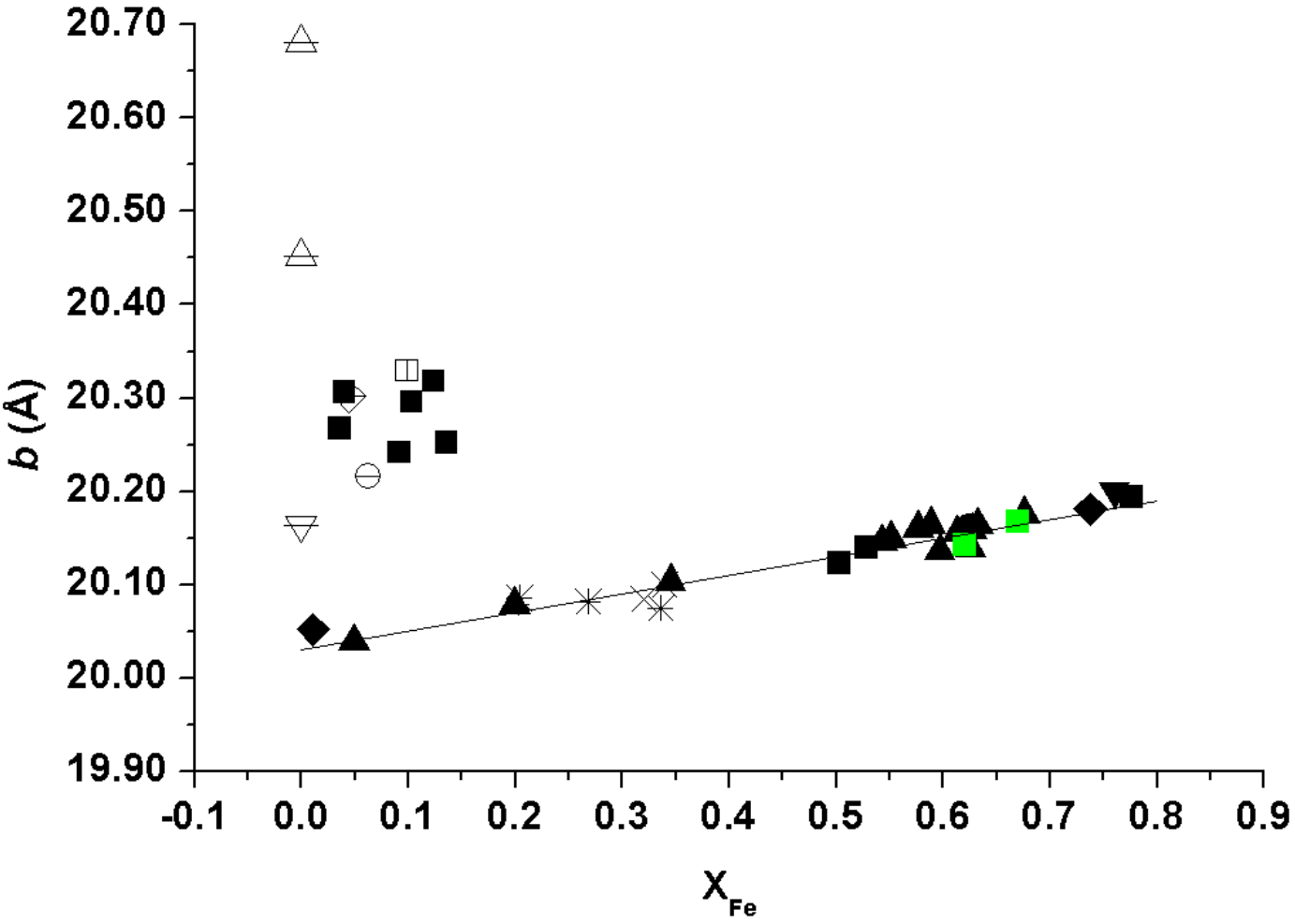

Fig 5b

This is the peer-reviewed, final accepted version for American Mineralogist, published by the Mineralogical Society of America.
The published version is subject to change. Cite as Authors (Year) Title. American Mineralogist, in press.
DOI: https://doi.org/10.2138/am-2020-7385. http://www.minsocam.org/

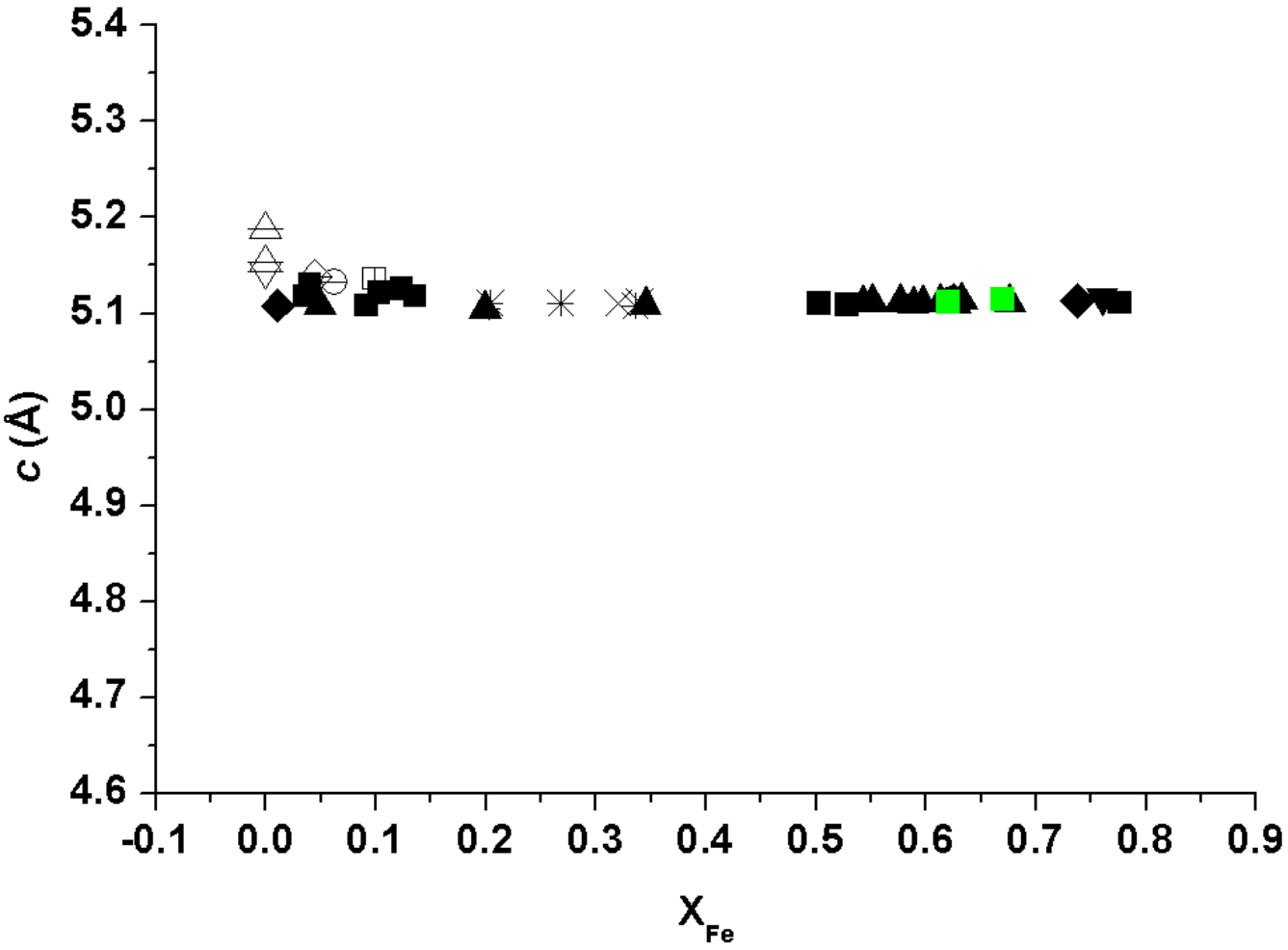

Fig 5c

This is the peer-reviewed, final accepted version for American Mineralogist, published by the Mineralogical Society of America.
The published version is subject to change. Cite as Authors (Year) Title. American Mineralogist, in press.
DOI: https://doi.org/10.2138/am-2020-7385. http://www.minsocam.org/

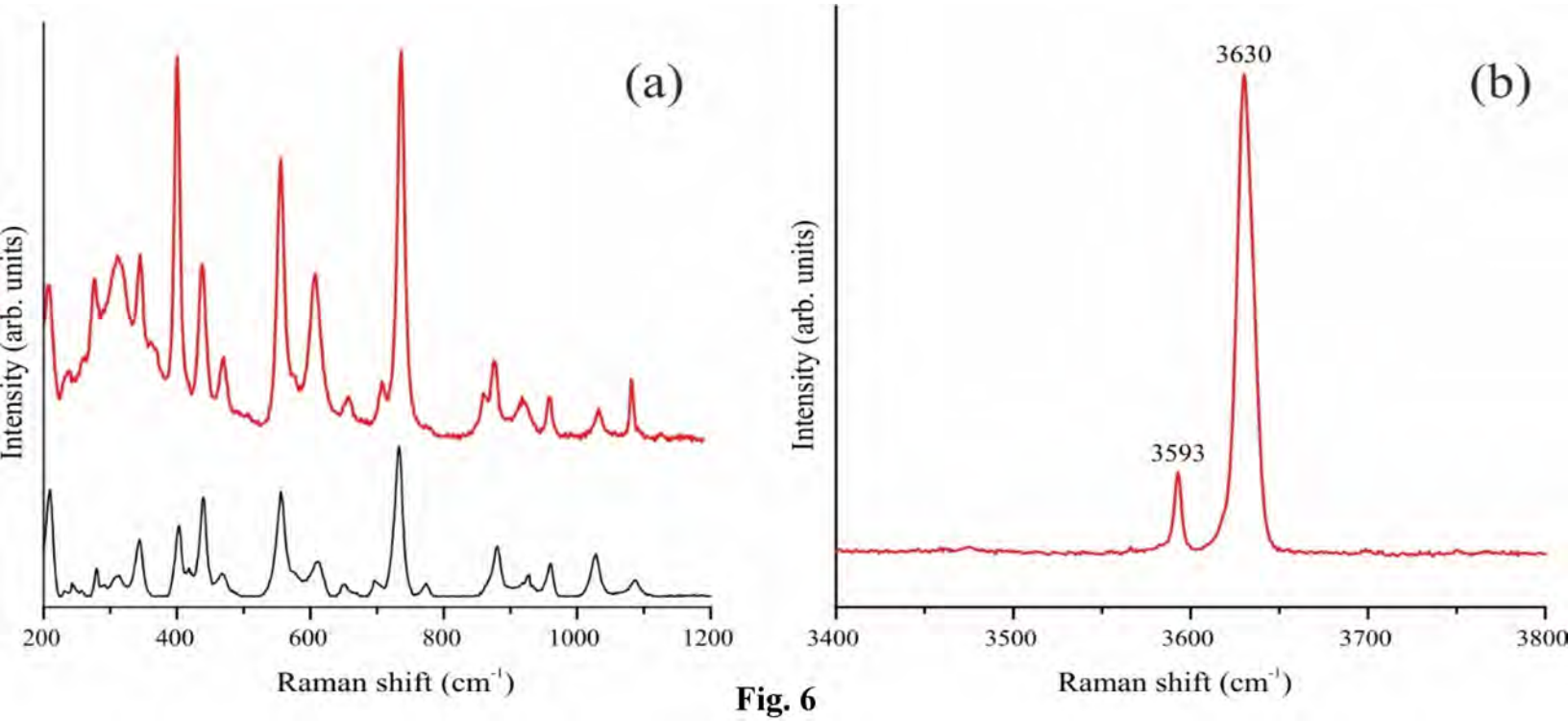

Fig. 6

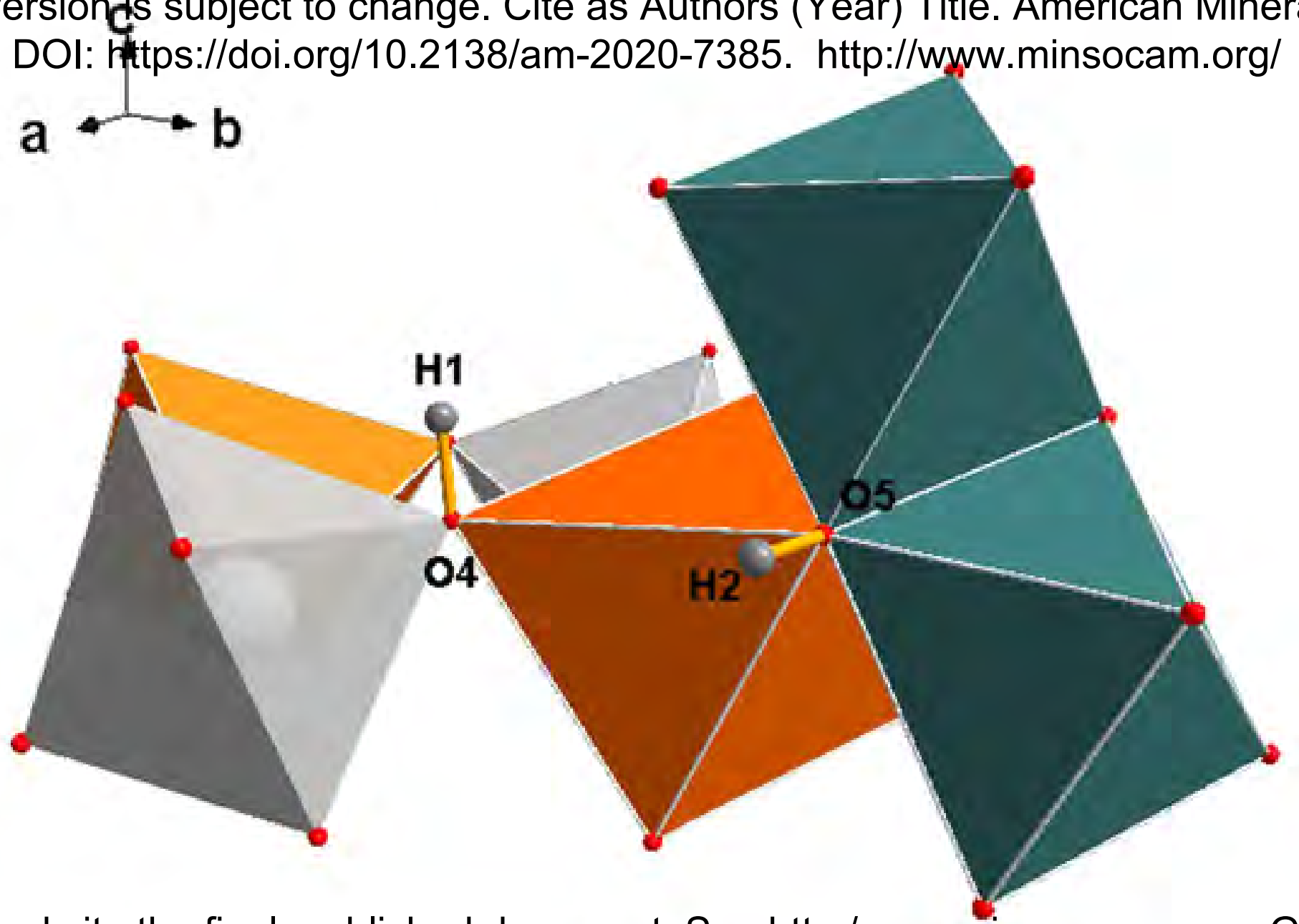

Fig 7

This is the peer-reviewed, final accepted version for American Mineralogist, published by the Mineralogical Society of America.
The published version is subject to change. Cite as Authors (Year) Title. American Mineralogist, in press.
DOI: https://doi.org/10.2138/am-2020-7385. http://www.minsocam.org/

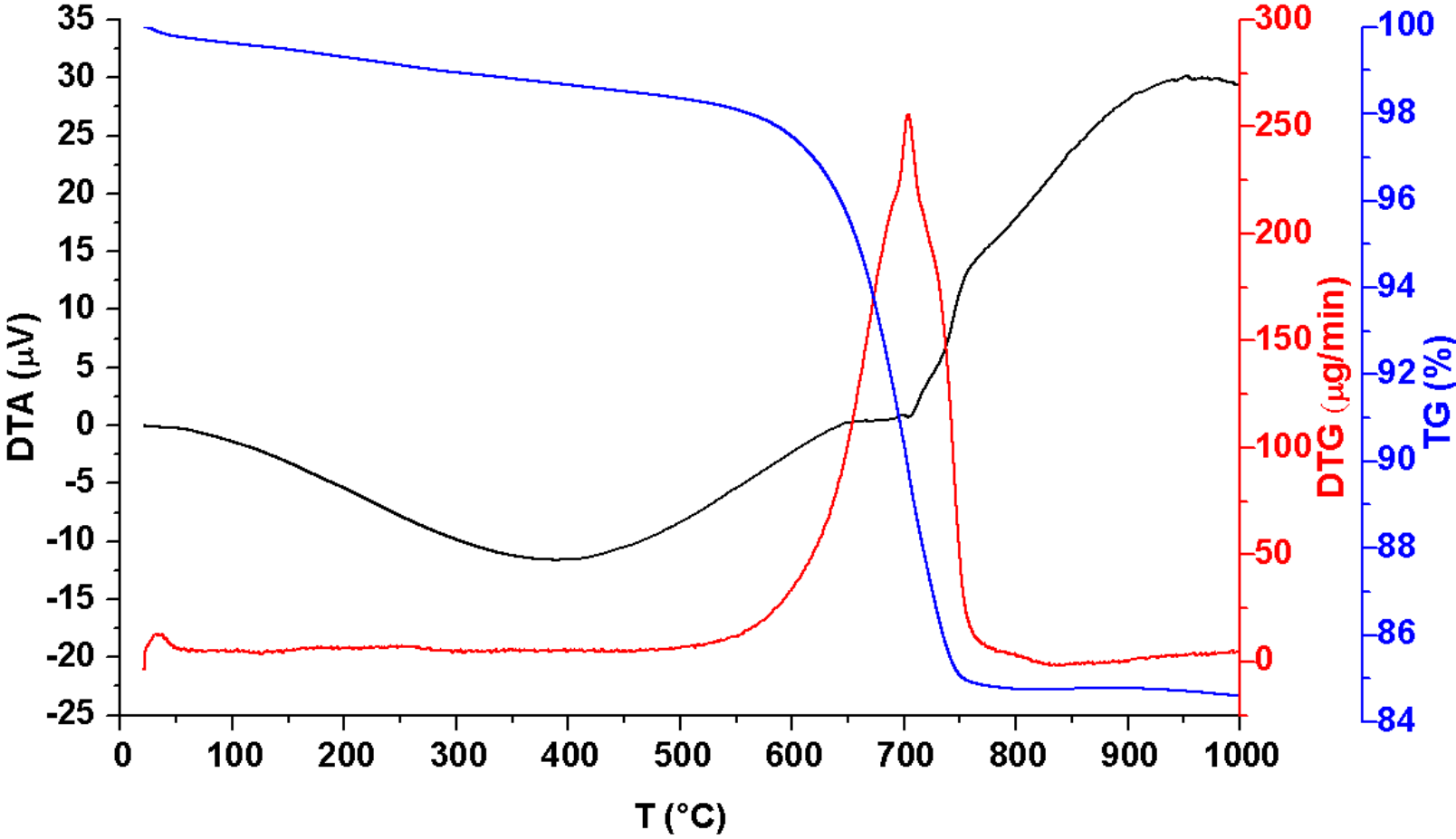

Fig 8

This is the peer-reviewed, final accepted version for American Mineralogist, published by the Mineralogical Society of America.
The published version is subject to change. Cite as Authors (Year) Title. American Mineralogist, in press.
DOI: https://doi.org/10.2138/am-2020-7385. http://www.minsocam.org/

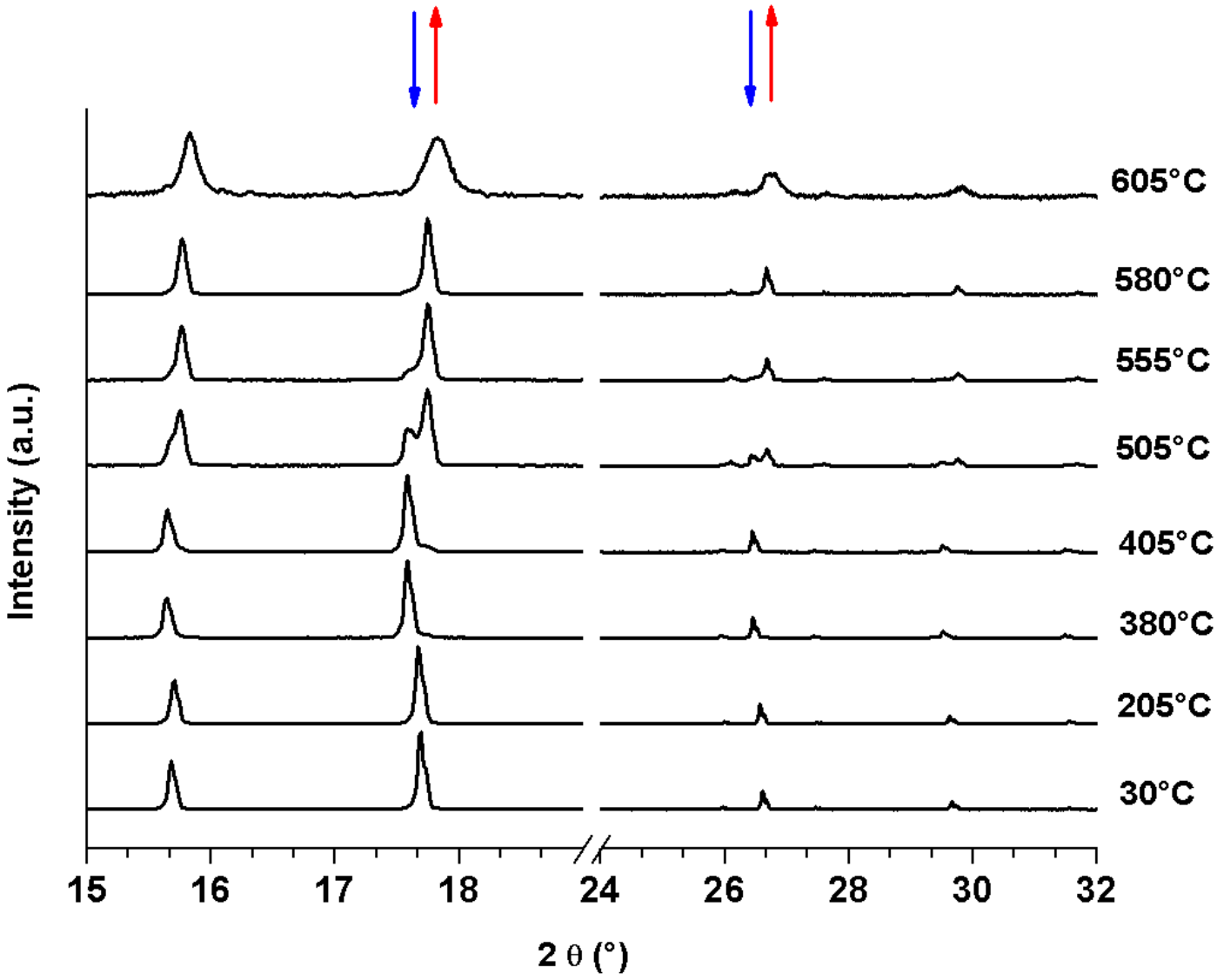

Fig 9a

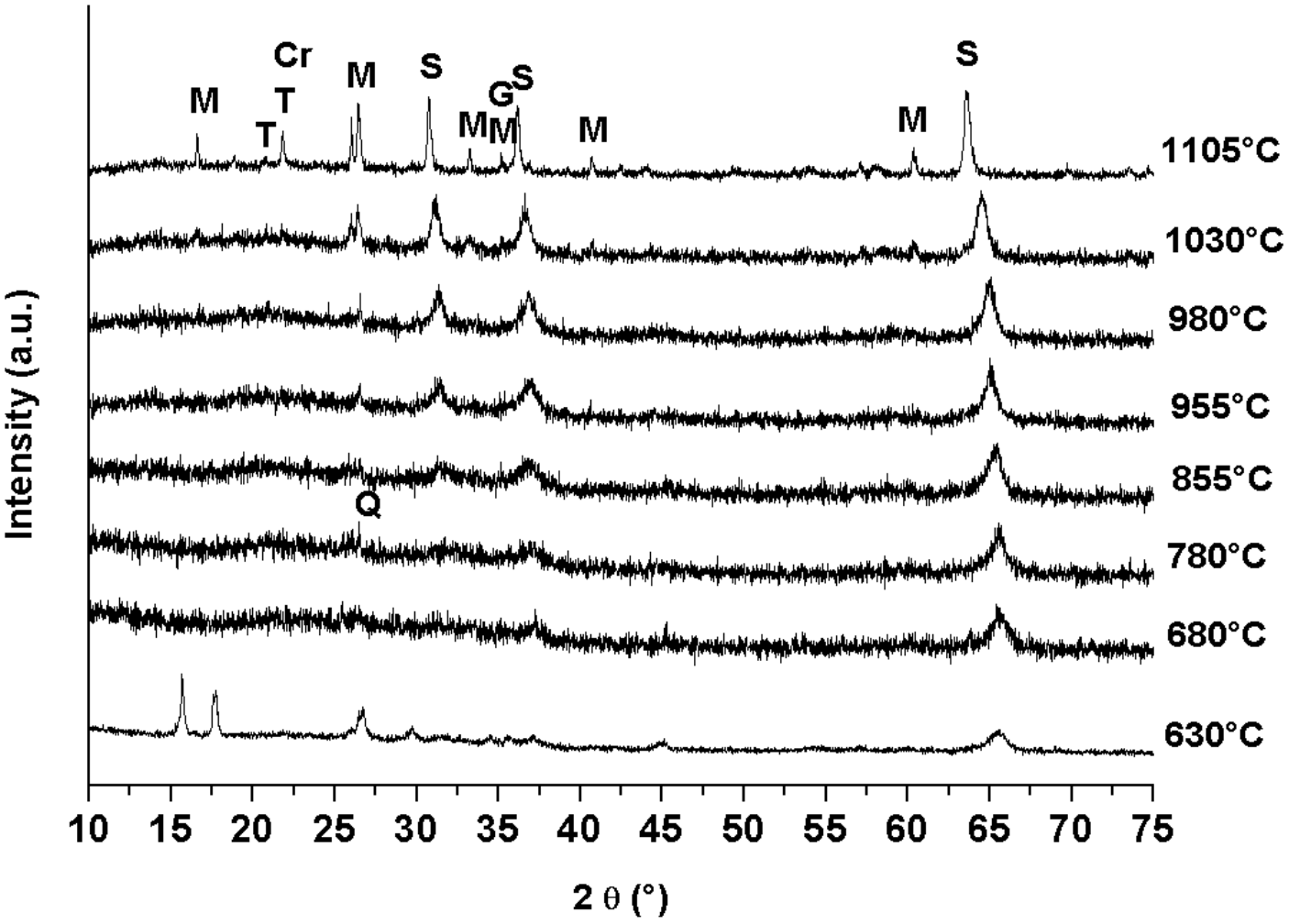

Fig 9b

This is the peer-reviewed, final accepted version for American Mineralogist, published by the Mineralogical Society of America.
The published version is subject to change. Cite as Authors (Year) Title. American Mineralogist, in press.
DOI: https://doi.org/10.2138/am-2020-7385. http://www.minsocam.org/

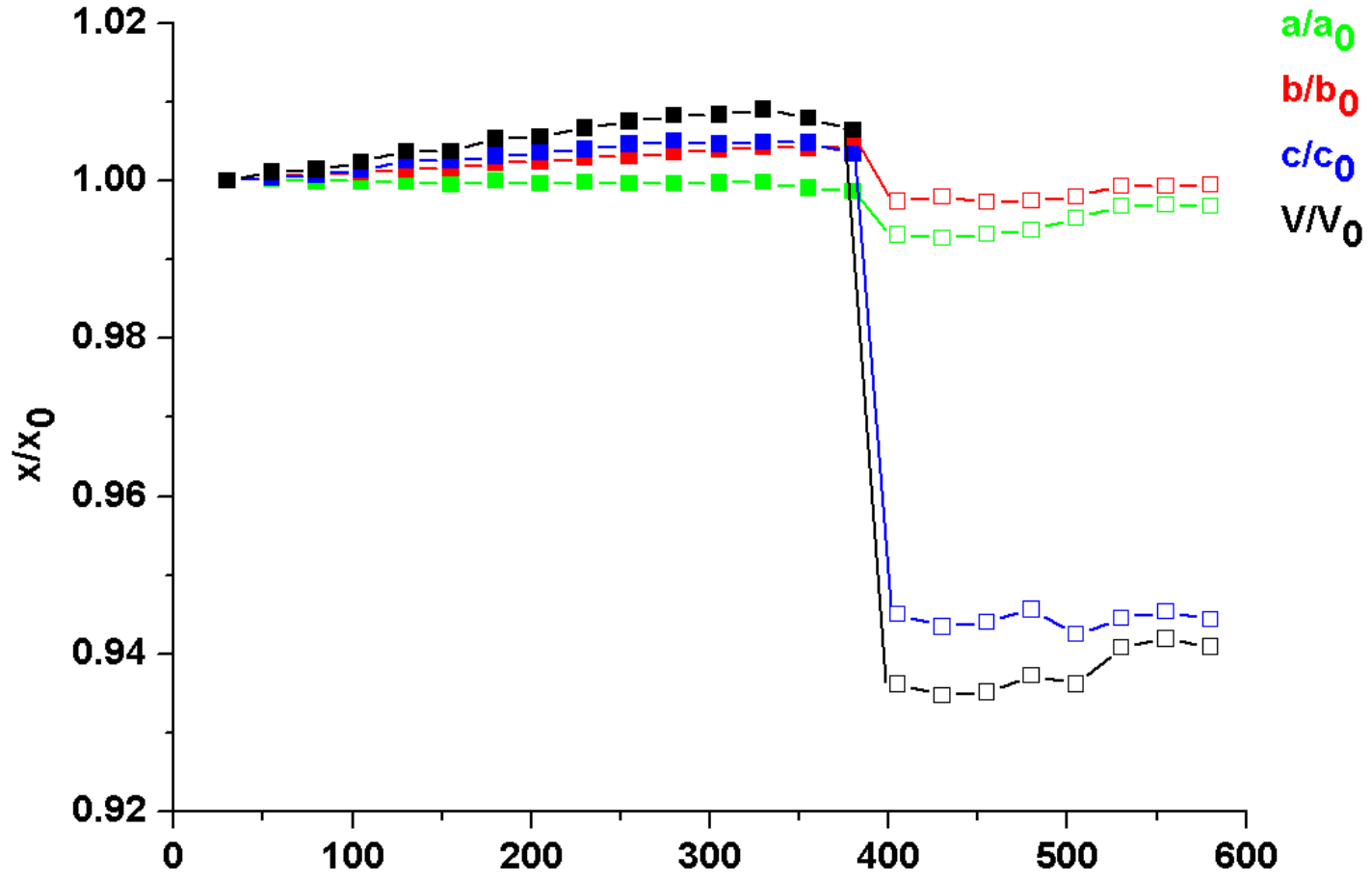

Fig. 10

This is the peer-reviewed, final accepted version for American Mineralogist, published by the Mineralogical Society of America.
The published version is subject to change. Cite as Authors (Year) Title. American Mineralogist, in press.
DOI: https://doi.org/10.2138/am-2020-7385. http://www.minsocam.org/

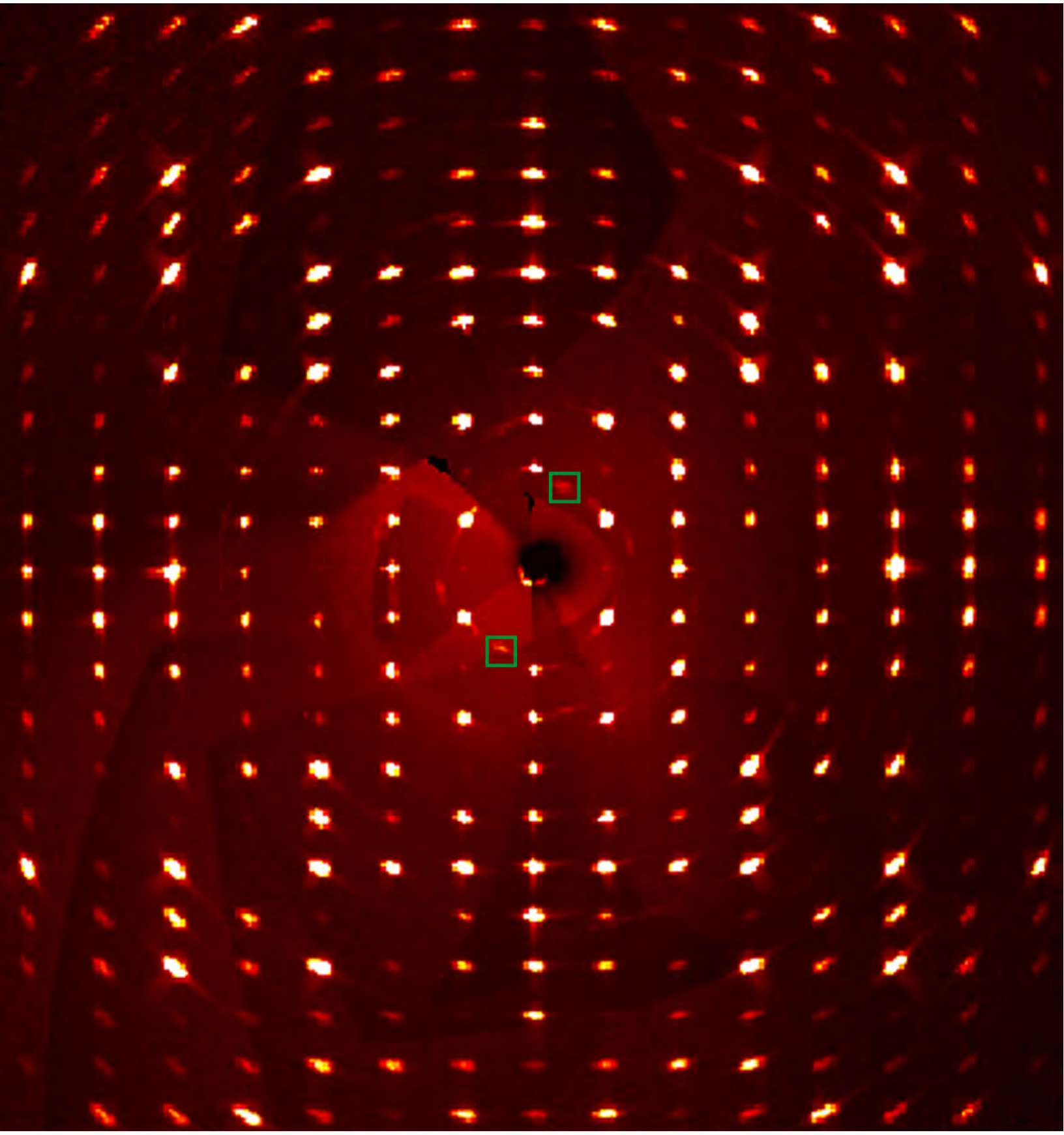

Fig. S1a

This is the peer-reviewed, final accepted version for American Mineralogist, published by the Mineralogical Society of America.
The published version is subject to change. Cite as Authors (Year) Title. American Mineralogist, in press.
DOI: https://doi.org/10.2138/am-2020-7385. http://www.minsocam.org/

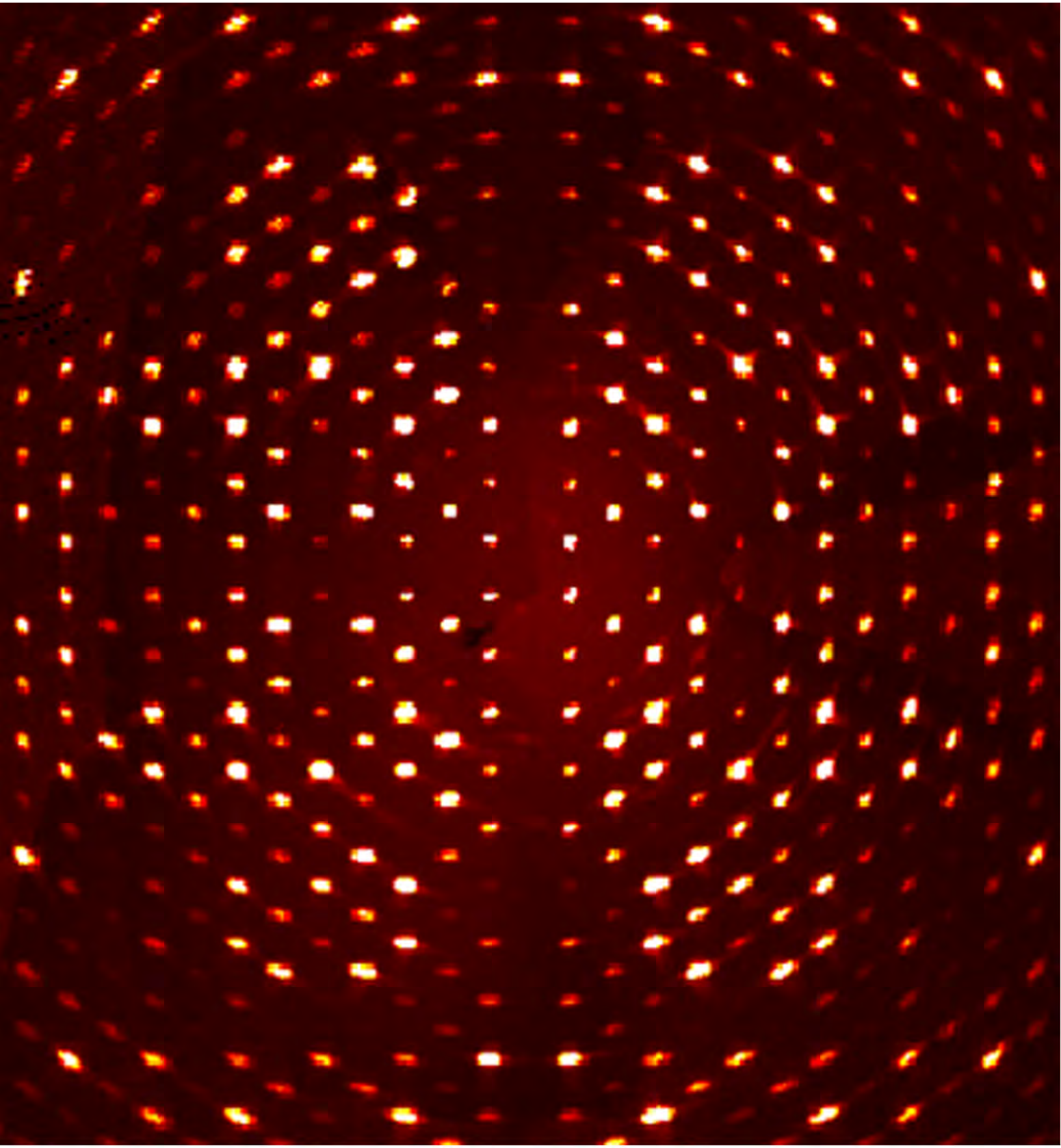

Fig. S1b

This is the peer-reviewed, final accepted version for American Mineralogist, published by the Mineralogical Society of America.
The published version is subject to change. Cite as Authors (Year) Title. American Mineralogist, in press.
DOI: https://doi.org/10.2138/am-2020-7385. http://www.minsocam.org/

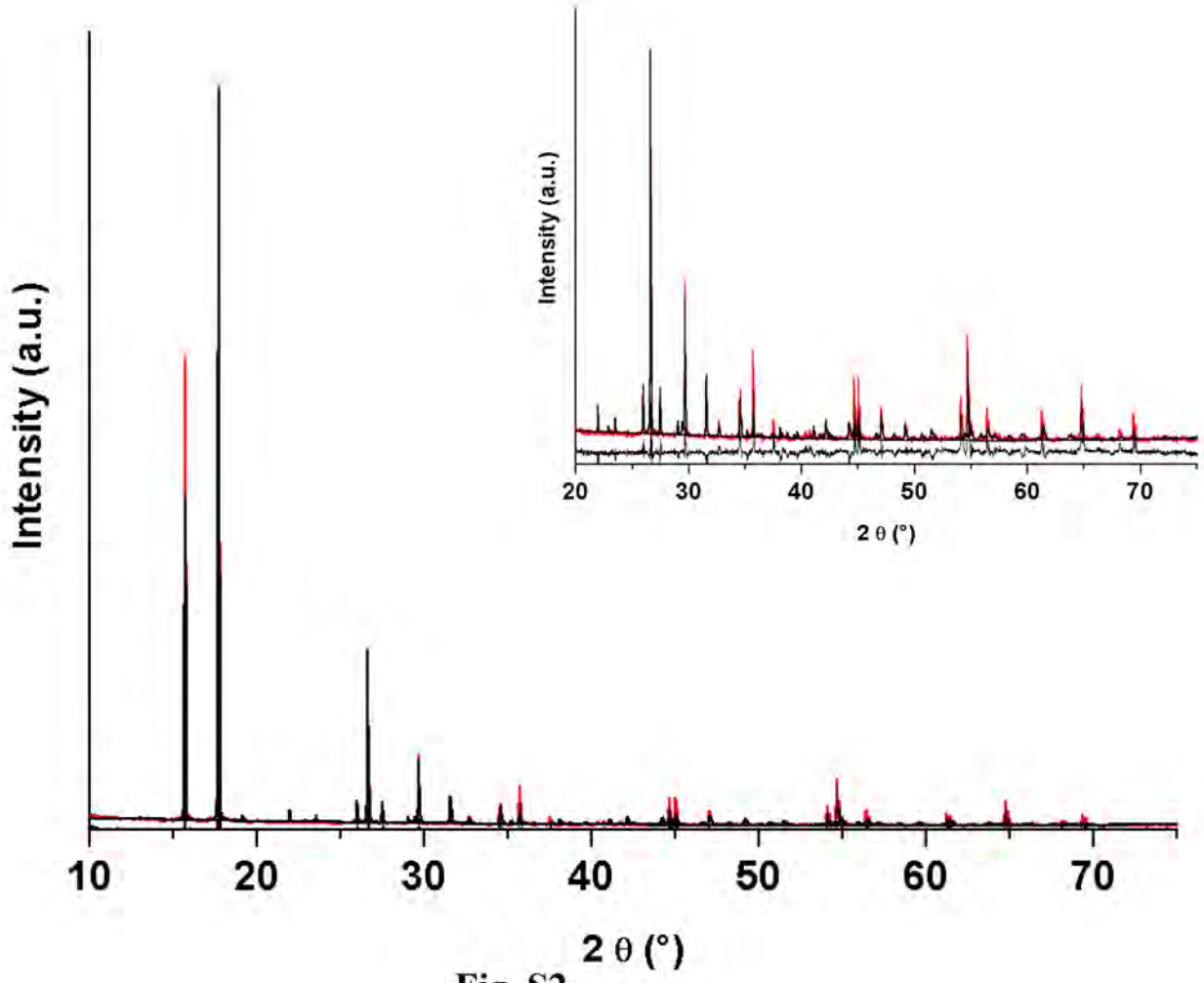

Fig. S2